University of Alberta
Printing Department

THE UNIVERSITY OF ALBERTA

THE EXCITED STATES OF BORON-10

by

ALISTAIR ANGUS FIFE

A THESIS

SUBMITTED TO THE FACULTY OF GRADUATE STUDIES

IN PARTIAL FULFILLMENT OF THE REQUIREMENTS FOR THE DEGREE

OF MASTER OF SCIENCE

DEPARTMENT OF PHYSICS

EDMONTON, ALBERTA

AUGUST, 1966

UNIVERSITY OF ALBERTA

FACULTY OF GRADUATE STUDIES

The undersigned certify that they have read, and recommend to the Faculty of Graduate Studies for acceptance, a thesis entitled THE EXCITED STATES OF BORON-10, submitted by Alistair A. Fife in partial fulfillment of the requirements for the degree of Master of Science.

ABSTRACT

The reaction $^{9}Be(d,n)^{10}B$ has been studied by time-of-flight techniques at bombarding energies of 3.5, 3.5, and 5.5 MeV. Contaminant neutron peaks due to the $^{16}O(d,n)^{17}F$ reaction were subtracted from the ^{10}B spectra at 5.5 MeV deuteron energy. Sixteen levels of ^{10}B were identified up to 7.56 MeV excitation, but no significant evidence was found for reported states at 5.18, 5.58, 6.40, 6.77 MeV. The DWBA theory was used to interpret the angular distributions for ℓ-values and spectroscopic factors, and plane wave theory was used in cases where the ^{10}B levels become unbound to proton emission. The angular distributions for the states at 3.59, 4.77, and 6.03 MeV could not be satisfactorily described by the DWBA theory. The spectroscopic factors were found to depend most sensitively on optical model parameter uncertainties, and also on whether or not finite-range and non-local effects were included.

Finally in an appendix, is a description of the use of the neutron time-of-flight system to measure target thickness.

ACKNOWLEDGEMENTS

I would like firstly to thank my supervisor Dr. G. C. Neilson for suggesting this topic of research and for his enthusiasm and constant encouragement which helped considerably towards its completion.

I am grateful for the cheerful participation of Dr. J. MacDonald in many aspects of this work and for his expert advice on the time-of-flight system.

I would like to thank Drs. W. G. Davies, W. K. Dawson for their assistance in running the DWBA code and for considerable advice on problems of data analysis. I am grateful to Mr. J. F. Easton for effective help rendered in this area. I take this opportunity of thanking Dr. Hird of the University of Manitoba for sending an amended version of the DWBA program.

I thank Dr. P. C. Sood for fruitful discussions of the $^{9}Be(d,n)^{10}B$ reaction.

I am particularly indebted to Mr. T. B. Grandy who has generously given his time and advice on many aspects of data collection and analysis. The assistance of Messrs. D. A. Gedcke, T. S. Lam, M. B. Burbank, A. W. Obst is also greatly appreciated.

I extend my sincere gratitude for the support of the technical staff of the University of Alberta Nuclear Research Centre, Messrs. J. B. Elliott, L. Holm, C. Green, R. Popik, P. Karvonen.

I thank Mrs. Medford for her meticulous and painstaking efforts in

TABLE OF CONTENTS

FIGURES

TABLES

CHAPTER I. MOTIVATION AND THEORY

1.1 Introduction

This thesis reports some time-of-flight studies of ^{10}B states excited via the deuteron stripping reaction $^{9}Be(d,n)^{10}B$, at bombarding energies of 3.0, 3.5, and 5.5 MeV. The purpose behind these studies was to clarify the existence of several weakly excited states previously reported for ^{10}B, and to obtain spectroscopic information for some of the more highly excited states, notably those at 6.14, 6.57, 6.88, and 7.00 MeV.

The weak states of interest have been reported at excitations of 5.18, 5.58, 6.40 and 6.77 MeV. We shall briefly survey the existing evidence.

The 5.18 level, one of the triplet of states between excitations of 5.10 MeV and 5.20 MeV, was initially interpreted from the reactions $^{6}Li(\alpha,\gamma)^{10}B$ [1], $^{6}Li(\alpha,\alpha)^{6}Li$ [2], and $^{9}Be(p,\gamma)^{10}B$ [3]. With a centre-of-mass width estimated at (110 ± 10)keV [4], observation of this state is difficult although it has been confirmed in (d,n) studies at 3 MeV [5].

The level at 5.58 MeV has been observed in (d,n) work by Ajzenberg [6], Hjalmar [7], and in a (p,γ) experiment by Singh [8], but the majority of evidence is negative [2,5,9-15]. In later high-resolution (p,γ) studies [16], γ-transitions associated with this level were not detected.

The level at 6.77 MeV has been observed in (d,n) work only [6], and its existence is largely discredited [9,13,17].

The 6.40 MeV level has been the subject of some controversy, positive evidence being obtained mainly from the $^{9}Be(d,n)^{10}B$ reaction [6,7,9,15]. There has also been a positive result from the $^{7}Li(\alpha,n)^{10}B$ reaction [18]. On the other hand a variety of reactions leading to ^{10}B states have yielded no trace of this level.

(i) $^{9}Be(^{3}He,d)^{10}B$ [14,17]

(ii) $^{10}B(d,d')^{10}B^{*}$ [12]

(iii) $^{10}B(p,p')^{10}B^{*}$ [12]

(iv) $^{11}B(^{3}He,\alpha)^{10}B$ [11,13,19,20]

(v) $^{6}Li(\alpha,\alpha)^{6}Li$ [2,21].

It must be pointed out that ^{16}O target contamination can give rise to spurious lines in the ^{10}B spectra. For example, neutrons from the $^{16}O(d,n)^{17}F$ reaction can contaminate forward angle neutron peaks corresponding to ^{10}B states at 5.93 MeV and 6.40 MeV. The ^{17}F state at 0.5 MeV excitation has an $l_p = 0$ angular distribution of neutrons whose centre-of-mass energies approximately correspond to those from the ^{10}B state at 6.40 MeV. In the experiments described here, the contributions to the ^{10}B spectra from the $^{16}O(d,n)^{17}F$ reaction were estimated by separate measurements using an oxygen-16 target.

1.2 Theory

The plane-wave (PWBA) and the distorted-wave (DWBA) treatments of the stripping reaction mechanism were both used to interpret the collected data. This section gives a description of the theory with some discussion of the validity of its use for light nuclei.

Stripping theory has undergone a process of increasing sophistication since the original plane-wave formulation of Butler [22]). Where the deuteron D-state and tensor forces are ignored, deuteron stripping is the most easily described of such rearrangement collisions.

In the case of (d,n) stripping*, Butler proposed that a measurement of the neutron angular distribution could indicate the orbital angular momentum transferred to the residual nucleus. This leads directly to the parity change in the reaction, and places restrictions on the spin of the final state. For a zero-spin target, the l-value measurement specifies the spin to within one unit.

With a reaction A(d,n)B, spin conservation requires that

$$\underline{J}_B = \underline{J}_A + \underline{l}_p + \underline{s}_p = \underline{J}_A + \underline{j}_p$$

$$\text{i.e.} \quad \left|\underline{J}_B - \underline{J}_A\right|_{\min} - 1/2 \leqslant l_p \leqslant J_A + J_B + 1/2,$$

where $\underline{J}_A$ = spin of target A,

$\underline{J}_B$ = spin of residual nucleus B,

$\underline{l}_p$ = orbital angular momentum transferred,

$\underline{s}_p$ = intrinsic spin of transferred proton,

$\underline{j}_p$ = total spin of transferred proton.

Parity conservation leads to the equation

$$\pi_B = \pi_A(-1)^{l_p}$$

---

*This discussion applies equally well to (d,p) stripping and also to the inverse pickup reactions.

where π_A = parity of the ground state of A,

π_B = parity of the final state of B.

Although the plane-wave theory enjoyed some initial success for light target nuclei, it failed to give the correct absolute cross-section, often overestimating the latter by an order of magnitude or more. The evidence collected from stripping on medium and heavy nuclei indicated that the PWBA was not wholly successful in these mass regions, often leading to ambiguous ℓ-value assignments. Coupled with this fact were indications that the simple theory did not give the correct dependence of the differential cross-sections on energy and Q-value.

The adaptation of the theory using the distorted waves Born approximation, and its subsequent application, has indicated that Coulomb and nuclear distortion effects are always important in stripping reactions. The plane-wave treatment is never a good approximation.

The DWBA theory allows for the scattering and absorption of the incident deuteron before stripping, and of the outgoing nucleon in the exit channel, by replacing the plane-waves of Butler's theory by elastic scattering waves. The latter are generated by Coulomb and optical model potentials which reproduce the measured elastic scattering from the same nucleus, at the same energy.

There have been many excellent reviews of the modern DWBA theory [23-26]) and only a brief résumé of the version used for the present calculations will be given.

The differential cross-section for A(d,n)B stripping can be written

as [24])

$$\frac{d\sigma}{d\omega} = \frac{1}{2} \frac{m_d m_n}{(2\pi\hbar^2)^2} \cdot \frac{k_n}{k_d} \cdot \frac{2J_B + 1}{2J_A + 1} \cdot C^2 \sum_{\ell,m,j} S_{j\ell} \, B_\ell^m{}^2$$

where m_d, m_n are the reduced masses of the deuteron and the neutron and k_d, k_n, their relative wave numbers. C is the Clebsch-Gordan isospin coefficient

$$\left\langle T_A \; t_p \; M_{T_A} \; m_{t_p} \middle| T_B \; M_{T_B} \right\rangle$$

B_ℓ^m is the stripping amplitude, calculated by numerical integration. Explicitly

$$B_\ell^m = \frac{(i)^{-\ell}}{\sqrt{2\ell+1}} \int \left[\chi_n^- (\underline{k}_n, \underline{r}_n)\right]^* \phi_\ell^m (\underline{r}_p) \, V_{np} \chi_d^+ (\underline{k}_d, \underline{r}_d) \, \phi_d (\underline{r}_{np}) \, d\underline{r}_p d\underline{r}_n$$

The $\chi(\underline{kr})$ are the elastic scattering wave functions for a pair of particles with relative momentum $\underline{k}$ and separation $\underline{r}$. The plus and minus refer to their asymptotic behaviour. ϕ_ℓ^m is the wave function of the proton bound to the target, and ϕ_d is the deuteron wave function.

The residual interaction responsible for the stripping transition is taken as V_{np}, the neutron-proton interaction. More accurately

$$V_{residual} = V_{np} + V_{nA} - V_{nB}$$

where V_{nA} is the neutron-target interaction and V_{nB} is the optical potential in the final channel. One usually approximates $V_{nA} = V_{nB}$ although this is not strictly true since V_{nA} is real and V_{nB} is usually complex. Additionally, off-diagonal elements of V_{nA} which correspond to target excitation do not cancel out, and one hence ignores contri-

butions from the two-step processes where the target nucleus is excited by inelastic scattering before stripping occurs.

Solutions for the radial parts of χ_d^+, χ_n^-, ϕ_ℓ^m, are generated numerically from the Schrodinger equation

$$F_\ell''(r) - \frac{2m}{\hbar^2}\left[E_{c.m.} + V_c(r) + V(r) - \frac{\hbar^2}{2m}\frac{\ell(\ell+1)}{r^2}\right]F_\ell(r) = 0 \qquad (1)$$

where $V_c(r)$ is the Coulomb potential and $V(r)$ the optical potential.

The six-dimensional integral for B_ℓ^m can be reduced to a three-dimensional form by using the zero-range approximation for V_{np}. One sets

$$V_{np}\cdot\phi_d = D_o^2\,\delta(r_{np})$$

where $D_o = 1.23 \times 10^2$ MeV.fm$^{3/2}$ and ϕ_d is the Hulthen wave function.

The zero-range approximation essentially means that the deuteron is absorbed at the same point the outgoing nucleon is produced.

The "local-energy " approximation [27]) allows one to relax the zero-range restriction and include a finite range for the n-p interaction. In the final analysis, this approximation includes the following correction factor in the three-dimensional integral for the zero-range case[28]) :

$$\Lambda(r) = \left(1 - \frac{\beta^2}{\alpha^2 B_d}\left(V_d(r) - V_n(r) - V_p\left(r\cdot\frac{M_A}{M_B}\right) - B_d\right)\right)$$

where $V_i(r)$ is the optical potential for particle i, B_d is the binding energy of the deuteron, and $\beta = 7\alpha$, with $\beta^{-1} = 0.6$ fm .

To account for the non-locality of nuclear forces, Perey[29]) has proposed that local wave functions (the type generated by equation (1)) be modified as follows:

$$\phi_{NL} = \left[1 + \frac{m\beta^2}{2\hbar^2} V_L(r) \right]^{-1/2} \phi_L$$

where ϕ_L, ϕ_{NL}, are the local and non-local wave functions respectively, $V_L(r)$ is the local optical potential, m is the reduced mass, and β is the range of the non-locality, usually about 1 fm.

Thus non-local and finite-range effects are included by multiplying the radial integrand of the zero-range case by four form factors.

1.3 Discussion of the Use of DWBA Theory for Light Nuclear Reactions

At this stage one can say that stripping reactions on medium and heavy nuclei for bombarding energies above the Coulomb barrier are reasonably well understood in terms of DWBA theory.

The stripping mechanism for light nuclei on the other hand, is not as clearly understood. In fact one can advance several reasons why one would not expect standard stripping theory to be very successful for light nuclei especially at low bombarding energies.

Some difficulties stem from compound nucleus effects which are important in light nuclei because of their lower level density. At low energies the compound nucleus can usually exist in a series of sharp states well separated in energy. If the energy spread in the incident beam is less than the mean level spacing then the scattering cross-section will show characteristic variations unaccounted for by the optical model.

Compound elastic scattering is indistinguishable from the direct shape elastic scattering described by the optical model. Hence optical parameters for low energy scattering in a light nuclear region may be in error. Also for very light nuclei, exchange reactions may take place sufficiently often to render the optical model invalid except for small scattering angles.

Inelastic neutron scattering will also contribute in cases where (d,n) stripping is being studied. It has been noted however [65], that despite strong fluctuations in differential cross-sections near a compound resonance, the angular shapes vary little. This may indicate that the competing compound amplitude for many reactions in light nuclei is small. In the latter studies of the $^{12}C(d,n)^{13}N$ reaction for energies 1.50 MeV to 3.00 MeV it was found that the shape of the angular distributions averaged over bombarding energy is probably given by the direct amplitude alone.

Statistical model (Hauser-Feshbach) calculations performed by Siemssen et al [49] for the $^{9}Be(d,n)^{10}B$ reaction at energies between 1.5 MeV and 3.0 MeV were not wholly successful. They concluded that the statistical model calculations either highly overestimated the compound amplitude, or that the statistical model was not valid for the open channels considered. In the light of these statements it was felt that no significant information could be gained by performing statistical model calculations for the $^{9}Be(d,n)^{10}B$ reaction at 5.5 MeV. A recent study [15] of the latter reaction at 7.00 MeV bombarding energy

where the appropriate optical parameters were known, indicated that the DWBA theory was moderately successful in reproducing the main stripping peaks, at least for transitions to the first four states of ^{10}B.

One of the difficulties of using DWBA theory for a reaction such as $^{9}Be(d,n)^{10}B$ is that the extreme j-j coupling model does not hold for very light nuclei. Generally above mass 16, j-j coupled wave functions are used in the stripping formulation. However it is known [66]) that the spin-coupling scheme changes from the L-S extreme at the beginning of the 1p-shell to the j-j form as the shell fills. Unfortunately, for most of the studied transitions more than one j-value is allowed from angular momentum conservation. Hence there is a chance that a mixture of different j-values will be present. In the calculations reported here, the extreme j-j coupling model was employed, and a single stripping amplitude allowed for in any one calculation.

CHAPTER II. EXPERIMENTAL DETAILS

2.1 Introduction

In fast neutron spectroscopy, the most precise measurement of neutron energy is by means of a time-of-flight spectrometer which determines the energies of neutrons by individually timing their flight over an accurately measured path. Since the amplitude of a signal from a neutron scintillation detector is rarely related to the particle energy in an unambiguous way, a pulse height distribution alone, is insufficient for neutron energy determination.

The basic function a time-of-flight spectrometer performs is to accurately fix two time points:

(i) the zero or start time of the neutron from the target

(ii) the time the neutron is detected at the end of the flight path.

From this time measurement, the neutron velocity is known and hence the energy.

These related time problems are best solved by pulsed beam technique which in recent years has developed into the most powerful method available for fast neutron spectroscopy in the nano-second time scale.

Beam pulses of short duration in comparison to the flight times to be measured, strike the target and initiate the reaction. The time zero signal marking the arrival of the ion burst at the target

is obtained by passing the particle beam through a hollow cylindrical capacitor before the target. The small charge pulse induced is amplified and appropriately shaped.

The corresponding stop signal is obtained from the neutron detector which usually consists of an organic scintillator optically coupled to a photomultiplier tube. The time between beam pulses is sufficiently long that the lowest energy neutron of interest can be detected before the arrival of the next pulse.

The start-stop pulses are then fed to a fast time-to-amplitude converter and the corresponding output signal analysed by a multichannel pulse height analyser.

The attractive features of the pulsed beam technique include high resolution, high detection efficiency and applicability to a wide range of neutron energies. The use of high-speed tunnel diode switching circuits has introduced considerable improvement in spectrometer resolution in the past few years. Improvements in beam pulsing techniques have also contributed.

In the next two sections, a description of the main experimental system is given. Section 2.2 deals with the essential features of the beam pulsing equipment installed in this laboratory, and section 2.3 describes the electronics associated with the time-of-flight spectrometer.

2.2 Beam Pulsing Equipment

The accelerator* and associated beam pulsing equipment delivered

---

*6.00 MeV Van de Graaff Accelerator, Model CN, High Voltage Engineering Corporation, Burlington, Massachussetts, U.S.A.

to the target assembly high intensity deuteron bursts of optimum pulse length 0.5 ns at a repetition rate of 1 MHz.

Several beam pulsing methods have been developed in the past:

(i) chopping the continuous ion beam from a Van de Graaff by means of a beam deflector and slit [30];

(ii) pulsing the ion beam before acceleration [31];

(iii) compression of the pulsed beam produced in (ii) after acceleration [32].

For deuterons of several MeV energy the most successful method is a combination of pre-acceleration pulsing and post-acceleration compression of this pulsed beam using a Mobley bunching magnet. High peak currents (~ma) can be obtained with very short pulse durations (< 1ns) and background radiation is much reduced over method (i).

Such a system has been installed at the University of Alberta Nuclear Research Centre and a simplified schematic of the equipment is given in fig. 1. A detailed treatment of this system with special emphasis on the theory of the Mobley magnet buncher can be found in the Ph.D. thesis of W.G. Davies[33]. A brief description only will be presented here.

At the high voltage Van de Graaff terminal, the R.F. ion source delivers a d.c. current of several milliamps of deuterons. The beam is focussed on a 1/16 inch aperture and swept across the aperture in an elliptical pattern by a pair of R.F. deflection plates set at right angles to each other in space, with the R.F. voltages 90° out of phase.

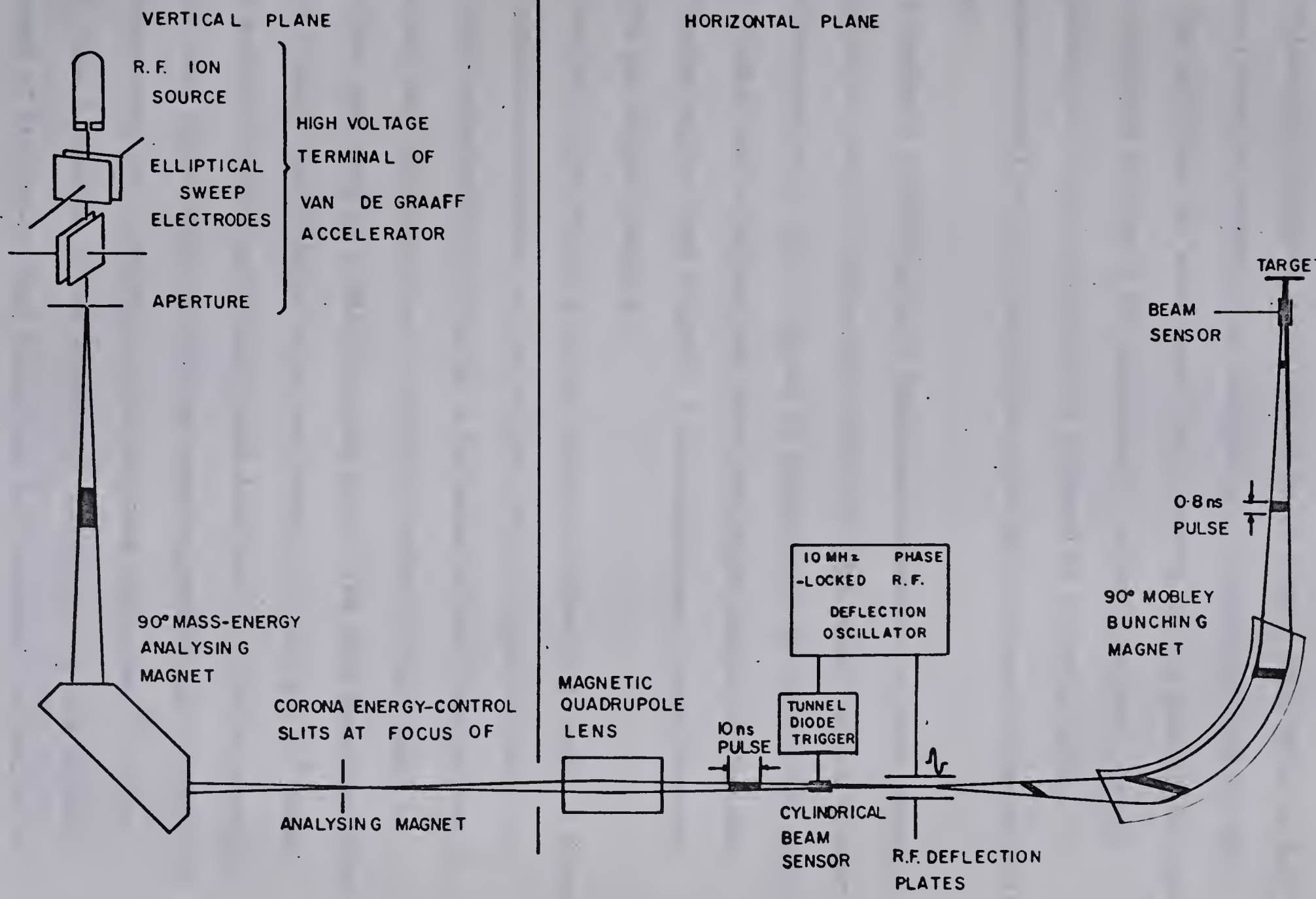

FIG 1 : ESSENTIAL FEATURES OF BEAM PULSING EQUIPMENT

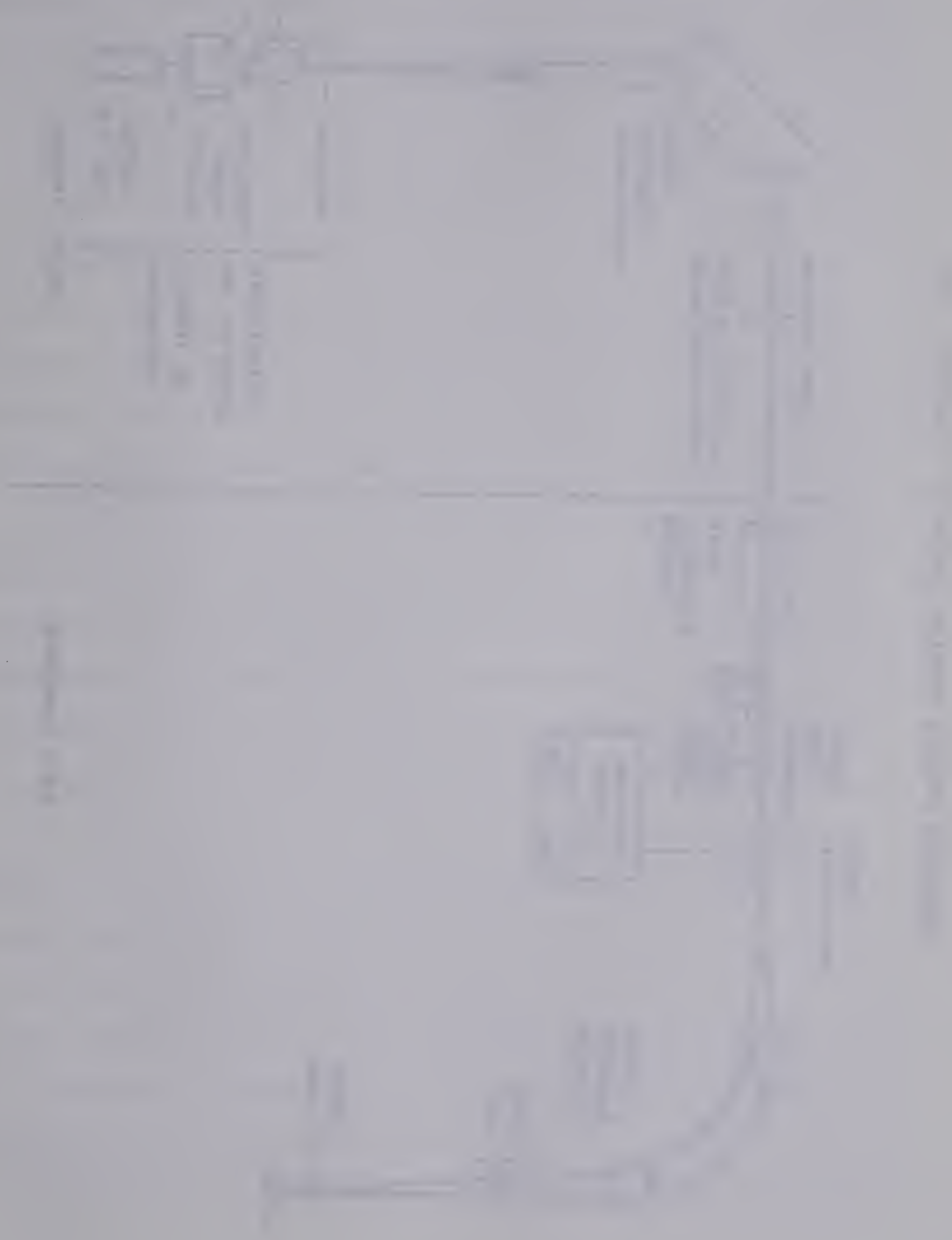

This pulsing kit produces a triangular pulse with a full-width at half-maximum (FWHM) of between 10ns and 15ns at a repetition rate of 1MHz.

The deuterons are accelerated and focussed at the accelerator base then refocussed through a 90° mass-energy analysing magnet. Energy stabilisation of the accelerator is achieved by a corona servo-mechanism controlled by signals from slits at the focus of the analysing magnet.

A magnetic quadrupole lens refocuses the beam at a point between the plates of the R.F. deflection system for the Mobley magnet buncher. Phase information of the ion pulse is supplied to the 10 MHz R.F. oscillator, from a hollow cylindrical electrode which surrounds the beam. A 90° Mobley magnet then delivers a time-compressed, space-focussed pulse to the target assembly.

The basic idea behind a Mobley bunching system is to apply a transverse momentum modulation to the initial 10ns ion pulse and then to sweep this deflected pulse through a suitable uniform field magnet in such a way that all particles in the pulse arrive at the target at almost the same time in a well-focussed spot. The beam bunching factor for the present installation is of the order of 12 using a 90° magnet with a radius of 75". An optimum pulse duration of 0.5ns is possible.

The main factor which limits the bunching performance in terms of time dispersion, is a property called the beam emittance [33]. The latter gives a measure of the transverse dimensions and the angular divergence of the pre-bunched pulse, and is a constant for motion in a

uniform magnetic field. Beam quality and the focussing properties of the quadrupole lens are the most significant factors governing the beam emittance.

2.3 Time-of-Flight Electronics

During the period in which part of this experimental work was carried out, a fast digital computer and memory display unit* became available, allowing large quantities of data to be processed within a reasonable time. Apart from the computer control of data collection, the main time-of-flight electronics used in the primary studies of the $^{9}Be(d,n)^{10}B$ reaction, were similar to the system operating under program control. Consequently the latter system will be described in this section.

The SDS 920 computer has 8192 24-bit words of memory of which 4096 are available for data storage. A cathode ray tube display unit operating under program control allows a two- or three-dimensional display of data collected in memory.

Connected on-line i.e. as a stored program multidimensional analyser [34,35], the computer allowed two major improvements to be made in the existing time-of-flight system.

1) The versatile general purpose kicksorter program (GPKS), written by Dr. W.K. Dawson could perform a real-time correction for time-shift [36] in the detection time of the fast signals from the neutron detector. A

---

*Scientific Data Systems 920, 1649 Seventeenth Street, Santa Monica, California.

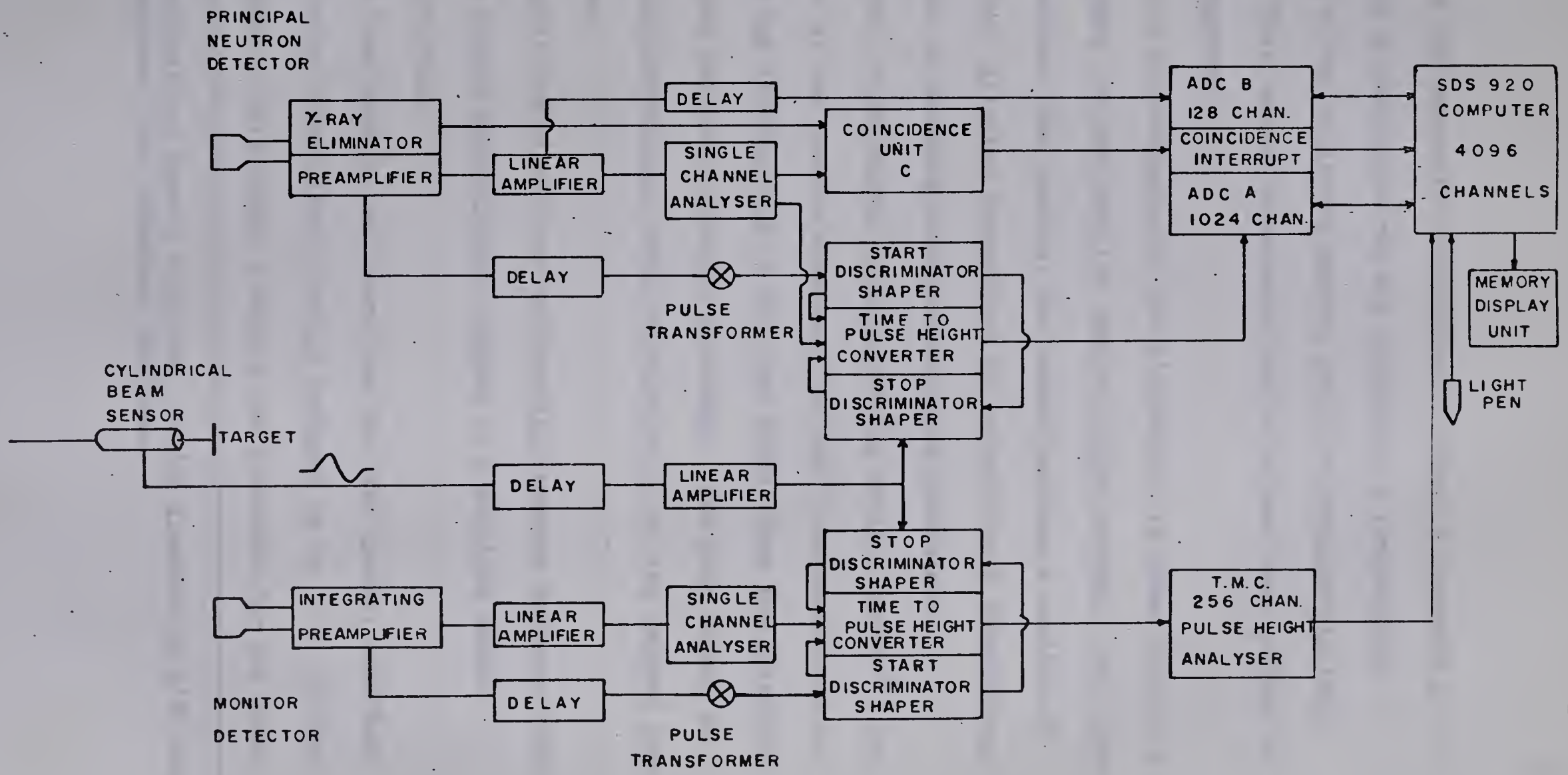

FIG.2. BLOCK DIAGRAM OF THE TIME-OF-FLIGHT ELECTRONICS

description of the time-shift correction is given in Appendix A.

2) Immediately a particular run was completed, a large-scale visual record of the collected spectra could be obtained via the c.r.t. unit. This enabled electronic drifts or poor beam quality to be quickly diagnosed.

A schematic block-diagram of the electronics is given by fig. 2. Essentially there are two parallel time-of-flight systems. The first records the neutron time spectra, the second provides a monitor of the first record, allowing corrections to be made for a fluctuating count rate, due to changing background or beam conditions.

Considerable experimental analysis of the on-line system[37]) has indicated that at low neutron energies, the best time-resolution is obtained when the leading edge of the fast signal from the principal neutron detector is used to specify time-zero. The stop signal is provided by the conventional cross-over detection of the delayed beam pick-off pulse.

Four signals are taken from the principal neutron detector which consists of a liquid scintillator* coupled to a Phillips XP1040 photomultiplier tube.

The fast time signals are taken from the 14th dynode, inverted, and fed to a start discriminator shaper designed by Dr. G.C. Neilson. The leading edge of this signal provides the time-zero for the time-

---

*Ne213 in a cylindrical quartz container, 3-1/2" diameter by 3/4" deep. Nuclear Enterprises, Ltd., Winnipeg, Manitoba.

to-amplitude converter (TAC) which is based on a design by D.L. Wieber [38]).

The stop signals for both time-of-flight systems are obtained from the cylindrical beam sensor located 30 cm before the target. This start-stop logic ensures that the stop discriminator will trigger only when a neutron is detected.

Signals from the anode and dynode 13 of the Phillips tube, provide the imput to a γ-n discriminator of the pulse-overlap variety [67]). Signals from dynode 12 have a three-fold purpose:

1. to provide a pulse height spectrum for the time-shift correction;
2. to provide a gate signal for the time-to-amplitude converter;
3. to provide a coincidence with the neutron signals from the γ-eliminator.

The pulse height spectrum is fed to a 128 channel analogue-to-digital converter (ADC B) and the output from the TAC to the 1024 channel converter ADC A.

With the time-shift correction, a system dead-time of the order of 700 μs allows GPKS to process a maximum of 1500 events per sec. During the time GPKS is storing an event, input to the computer is inhibited by the coincidence interrupt unit. The latter demands a triple coincidence between the following three signals before input to the SDS 920 occurs:

1. an address reset pulse from ADC A;
2. an address reset pulse from ADC B;
3. a logic pulse from coincidence unit C.

Signals 1,2 ensure that both ADC's accept amplitude pulses from the experiment only when both are free to do so, and signal 3 requires that the accepted pulses represent a true coincident pair. A logic pulse from the interrupt unit to the computer then indicates that the next two pulses on the data lines are to be treated as a coincident pair. A detailed description of this interrupt unit is contained in an internal report by D.A. Gedcke[39]).

The monitor detector consists of a 1" Naton phosphor* mounted on an RCA 8575 photomultiplier tube. The fast signals are taken from the anode, inverted, and detected in a fast tunnel diode cross-over pick-off circuit. The input to the TAC is gated by suitably shaped signals from the 13th dynode. Low-energy neutrons and γ-ray pulses are eliminated by a single-channel analyser.

The output from the monitor TAC is analysed and stored by a 256 channel pulse-height analyser, the contents of which can be later dumped into the computer memory under control of GPKS.

2.4 The $^{9}Be(d,n)^{10}B$ Reaction

Using the preceding time-of-flight system, this reaction was studied at three deuteron energies 3.00, 3.50, 5.54 MeV. The average current of deuterons on the target was between 2.0μa and 2.5μa. The ^{9}Be target consisted of a thin film of Beryllium metal vacuum deposited on a 1/32 inch thick Molybdenum foil. Various flight paths between 4.0m and 6.3m were used, but the majority of data was collected at a

*Nash and Thompson Ltd., Hookrise South, Tolworth, Surrey, England.

flight path of 6.3m and a deuteron energy of 5.54 MeV. For this deuteron energy data were collected at 5° intervals from 0° to 35°, and for 15° intervals from 45° to 150° (laboratory angles).

The experiments at 3.0 MeV, 3.5 MeV deuteron energy constituted a further search for the broad 5.18 MeV level of ^{10}B. For these energies measurements were made at the following laboratory angles: 0°, 15°, 30°, 45°, 60°.

2.5 The $^{16}O(d,n)^{17}F$ Reaction

With the purpose of estimating the contribution of this reaction to the $^{9}B(d,n)^{10}B$ spectra at 5.54 MeV, a separate study of this reaction was carried out using an oxygen-16 target. The latter consisted of a thin film of tantalum pentoxide (Ta_2O_5), deposited on a tantalum foil. As far as possible, experimental conditions were the same as those used for the $^{9}Be(d,n)^{10}B$ reaction at 5.54 MeV, and measurements were made at the same laboratory angles. As a check against the similarity of the two experiments, data for the $^{9}Be(d,n)^{10}B$ reaction were collected at the same time, for laboratory angles of 0° to 45° inclusive.

CHAPTER III. DATA ANALYSIS

3.1 Introduction

The analysis and interpretation of the collected data can be divided into two parts. The first part contained in Chapter III deals with the reduction of the raw $^{9}Be(d,n)^{10}B$ spectra to yield ^{10}B excitations and relative angular distributions of neutrons. The second part described in Chapter IV, presents evidence for the four weak states under study and describes the interpretation of the neutron distributions for ℓ-values and spectroscopic factors using plane-wave, and distorted wave theories of stripping.

A typical $^{9}Be(d,n)^{10}B$ spectrum for 5.54 MeV deuteron energy is indicated in fig. 3. The range of neutron energy covered by this spectrum is from about 1.5 MeV at the neutron cut-off, to 10 MeV, corresponding to the ground state of ^{10}B. For these spectra an overall time resolution of 1.3 ns was achieved, corresponding to an energy resolution of 85 keV for 6 MeV neutrons over a 6.3 m flight path. At this energy, sixteen neutron groups were identified corresponding to ^{10}B excitations up to 7.56 MeV.

The data at 3.0 MeV, 3.5 MeV were collected after the neutron and γ-ray background had been reduced with additional shielding. A much improved time resolution of 0.85 ns was achieved corresponding to an energy resolution of about 50 keV for 6 MeV neutrons over a 6.3 flight

path. A 3.0 MeV spectrum for a laboratory angle of 15° is indicated in fig. 4.

3.2 Extraction of ^{10}B Excitations and Relative Angular Distributions

Due to the considerable quantities of data collected in present day nuclear physics experiments, reduction to meaningful information requires the use of fast computers, if the analysis is to be completed in a reasonable time.

A flow diagram for the data analysis of these experiments is presented in fig. 5. In all, eight separate computer programs were employed, the majority of which were written in this laboratory.

The initial task was identification of known neutron peaks in the spectra using a relativistic kinematics program written by T.B. Grandy. From the known excitations and bombarding energies the program supplied the corresponding neutron flight times for a 6.3 m flight path, thus enabling a time scale to be constructed for each spectrum. The times for the unknown peaks could then be found.

The program involved with the estimation of the mean ^{10}B excitations and the Gaussian analysis of the spectral peaks were written by W.G. Davies, and are fully reported in his Ph.D. thesis [33].

Firstly, a general purpose least-squares program was employed to fit a linear or quadratic time calibration line for all the spectra, using the times for the known peaks. This line was computed at all angles because at some angles slight differences were introduced by electronic drifts.

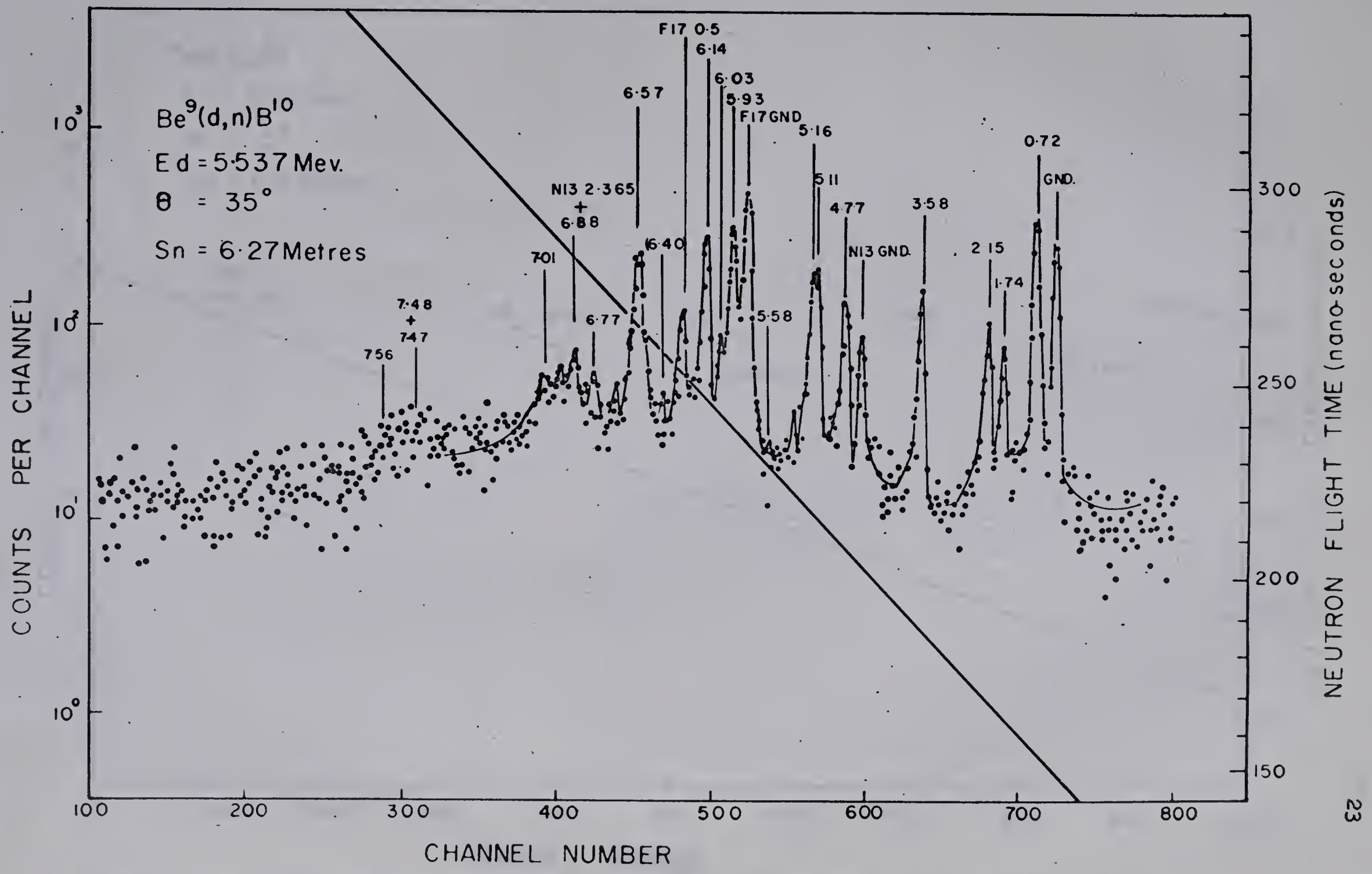

FIG.3. TIME-OF-FLIGHT SPECTRUM FOR $^{9}BE(d,n)^{10}B$ REACTION AT E_d=5.537MeV, θ_{lab} = 35°.

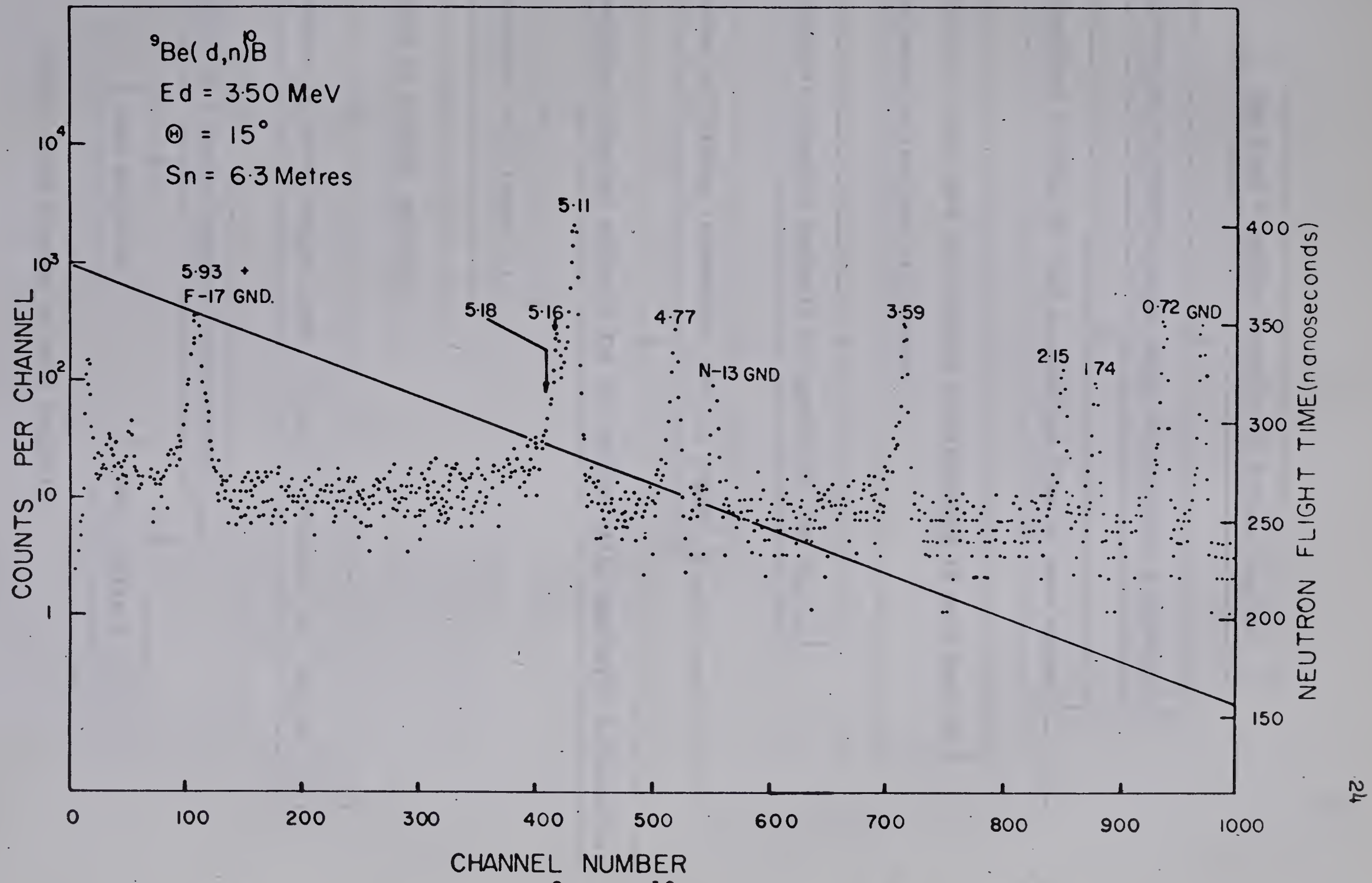

FIG.4. TIME-OF-FLIGHT SPECTRUM FOR THE $^{9}Be(d,n)^{10}B$ REACTION AT E_d = 3.50MeV, θ_{lab} = 15°.

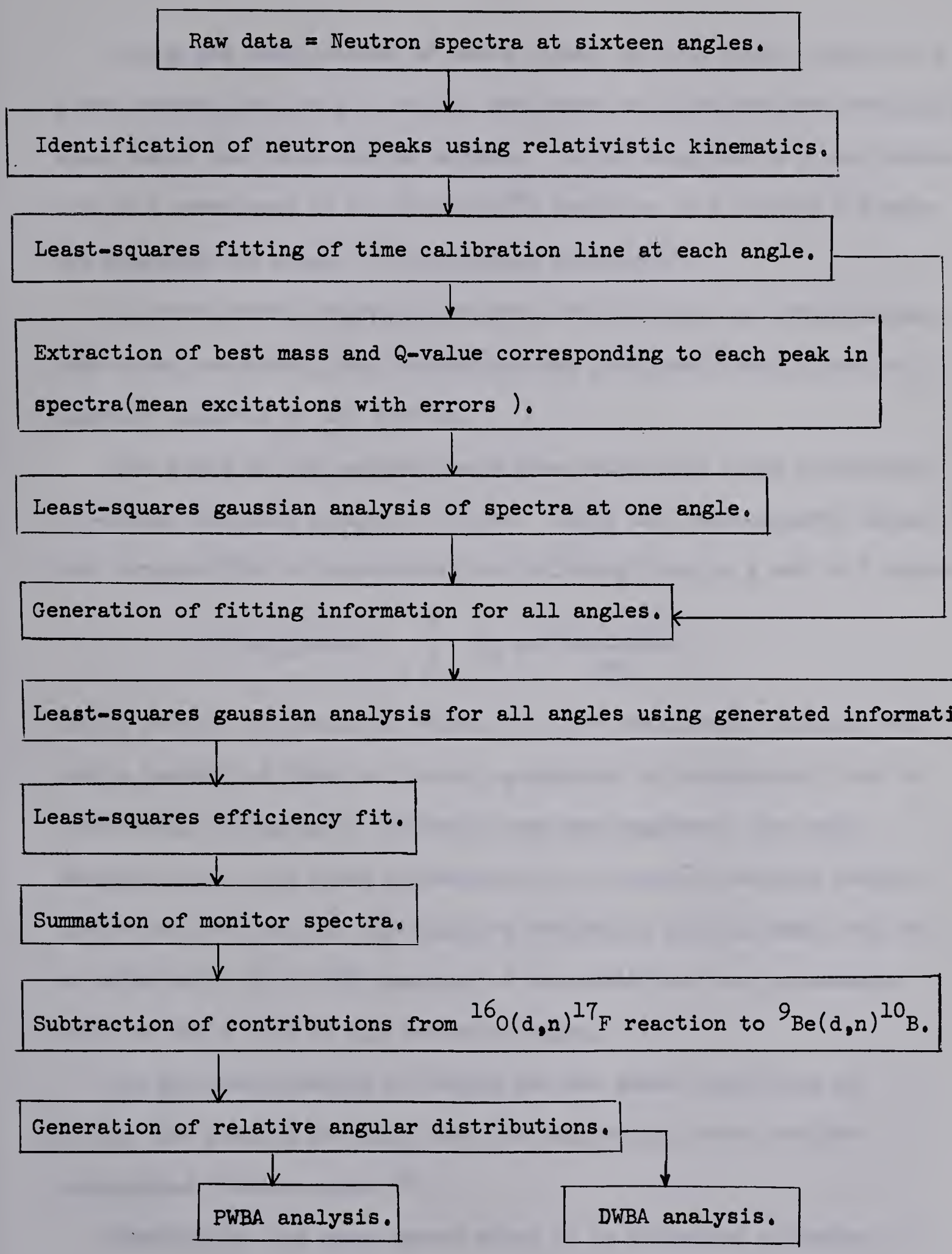

Fig.5. Flow diagram of data analysis.

Using the coefficients of these lines, and the flight times for a given neutron peak at all angles, best mass and Q-values were estimated again using the least squares method. On deciding that a given neutron peak did correspond to the $^{9}Be(d,n)^{10}B$ reaction, the correct ^{10}B mass was inserted and a mean ^{10}B excitation calculated.

In cases where neutron peaks were not resolved, or contaminated from other reactions, this estimation was postponed until after the Gaussian analysis of the spectra.

The areas of the neutron peaks were calculated using a weighted non-linear Gaussian analysis program. Using the least-squares method [33], this program fits a function of the following form to a set of N peaks:

$$y = \text{background} + \sum_{i=1}^{N} A_i \exp \frac{-(x - \bar{x}_i)^2}{2\sigma_i^2}$$

Here y denotes the count in channel x. The background function could have a variety of forms — linear, quadratic, or exponential,-but in practically all cases, a quadratic form was employed. For each Gaussian curve, the three parameters A_i, σ_i, and $\bar{x}_i$ denoting respectively the peak height, the standard deviation, and the mean, had to be estimated. Up to 100 channels of data with ten free parameters could be dealt with in any one calculation.

In the determination of errors for the above quantities A_i, σ_i, x_i, the program includes both the statistical error and the chi-squared fitting error [40].

Explicitly, the mean square error of an estimated parameter α_λ

(e.g. mean , standard deviation etc.) from its true value α_λ° is given by

$$\left\langle (\alpha_\lambda - \alpha_\lambda^\circ)^2 \right\rangle_{AV.} = \frac{\chi^2}{N - p} \cdot \sigma(\alpha_\lambda)^2$$

where (i) $\chi^2 = \Sigma_i W_i (\mu_i - \xi_i)^2$ with W_i the weight, μ_i the measured value on the Gaussian curve, and ξ_i the theoretically estimated value;

(ii) N is the number of measurements and p is the number of free parameters;

(iii) $\left(\sigma(\alpha_\lambda)\right)^2$ is the mean-square deviation in α_λ estimated from the least-squares analysis.

A comparison between the mean square error in α_λ and its mean-square deviation indicates the importance of non-statistical errors. If systematic errors can be ignored, a value of $\chi^2/(N-p)$ significantly greater than unity would imply that the Gaussian function used in the analysis is wrong.

The assumption of a Gaussian form for the spectral peak is open to some question, but in most cases this has proved to be a reasonable assumption. Peaks with large areas tended to be slightly asymmetrical, but the areas calculated using the program were always within 5% of the values calculated by other means, e.g. summation by hand with subtraction of a constant background. The danger of using the automatic method is that it may consistently under- or over-estimate the area thus introducing systematic errors. A better method has been described recently by Tepel [69].

The Gaussian fit for all peaks of interest at one angle supplied the fitting information (means, standard deviations etc.) which was then used to calculate the necessary fitting information for the other fifteen angles. With this control information, the estimation of peak areas etc. could be placed on a semi-automatic basis.

In order to calculate angular distributions using these peak areas, the efficiency of the principal neutron detector as a function of neutron energy had to be determined. This was done by studying the reaction $^{7}Li(p,n)^{7}Be$ for proton energies between 3.0 MeV and 5.0 MeV. At 0^{o}, this proton energy range gave rise to neutrons of energies between 1.31 MeV and 3.33 MeV. The neutrons were detected both by the principal neutron detector and a "flat-response" long counter of the McKibben type [41]. The detectors were placed side-by-side at the longest flight path available (6.3m), in such a position that they subtended the same angle with respect to the proton beam direction.

The long counter detects neutrons corresponding to the ground and first excited states of ^{7}Be. The excited state counts were removed from the total, by dividing by the ratio $(1 + I_1/I_0)$ measured by Bevington et al [42]. The total ground state counts detected by the principal neutron detector were then normalised to the corrected McKibben counts for each proton energy, and the resulting efficiency curve is indicated in fig. 6. The solid curve is a least-squares fit to the data using the function

$$\text{Efficiency} = A \left[\frac{E_n - E_o}{E_n}\right]^n \sigma np$$

The symbols A, E_o, n are parameters of the fit, and σ_{np} is the semi-empirical n-p total cross-section [43])

$$\sigma_{np} = 3\pi \left(1.206\ E_n + (-1.86 + 0.09415\ E_n + 0.0001307\ E_n^2)^2\right)^{-1}$$
$$+ \pi \left(1.206\ E_n + (0.4223 + 0.13\ E_n)^2\right)^{-1}$$

After a study of the monitor spectra taken at each angle it was decided to normalise the $^{9}Be(d,n)^{10}B$ spectral areas to the total counts in the first 200 monitor channels.

For those peaks free of contaminants, relative angular distributions were then calculated using a program written by T.B. Grandy. This program normalised the areas to the monitor sums and made corrections for the relative efficiency of the neutron detector and for neutron attenuation in the gold target backing (1/16" thick). The angular distribution program combines errors from the following sources:

1. statistical errors from fitting process
2. errors estimated for efficiency
3. errors in monitor sums.

In a manner exactly similar to the above description, relative angular distributions were obtained from the $^{16}O(d,n)^{17}F$ data, for neutron groups corresponding to the ground and first excited states of ^{17}F. The two angular distributions are shown in fig. 7.

Then, essentially by inverting the calculations in the angular distribution analysis, the actual neutron contributions to the $^{9}Be(d,n)^{10}B$ spectra from the $^{16}O(d,n)^{17}F$ reaction were estimated.

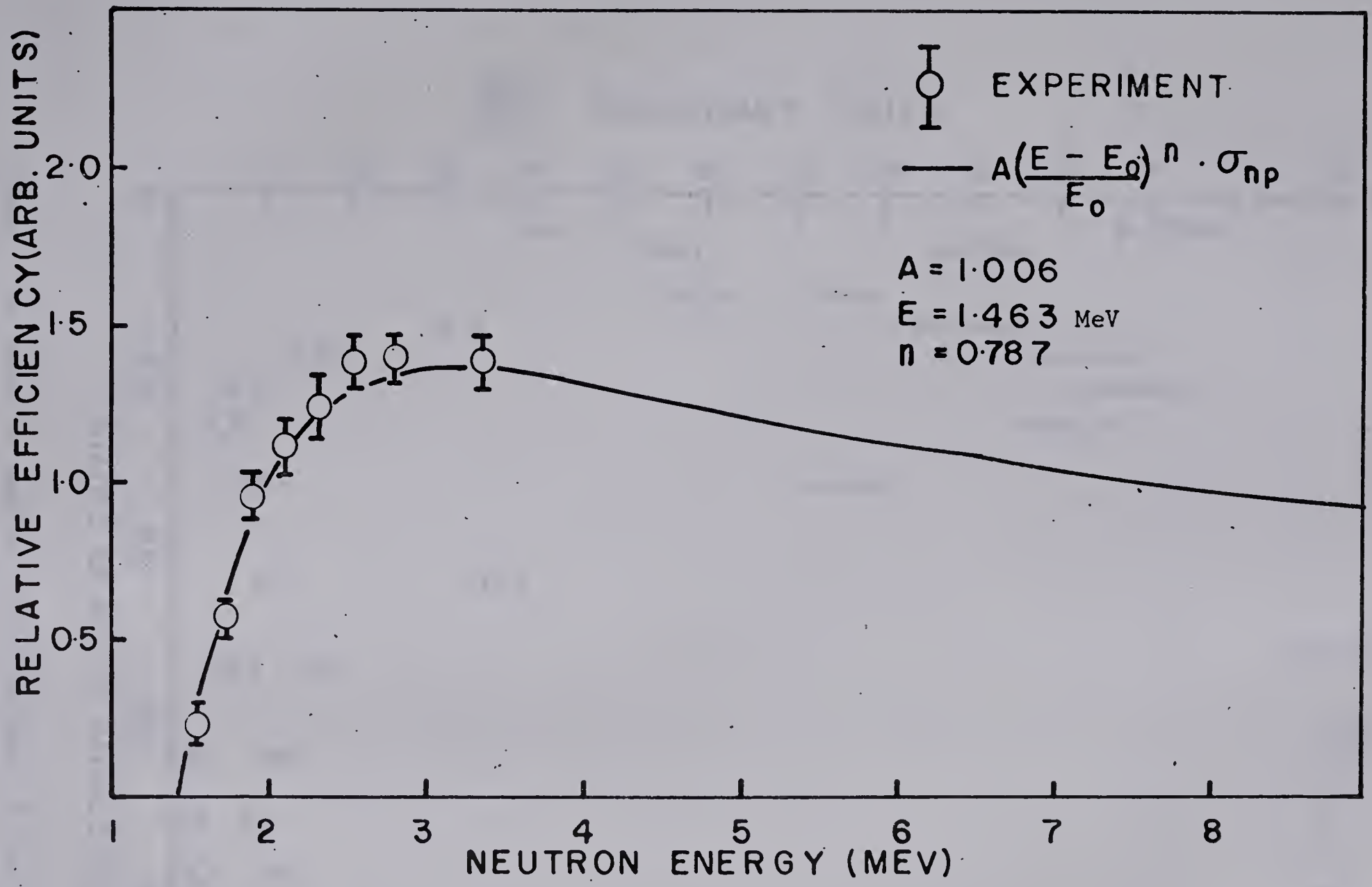

FIG.6 THE RELATIVE EFFICIENCY OF THE NEUTRON DETECTOR. THE SMOOTH CURVE IS A LEAST-SQUARES FIT TO THE DATA USING THE INDICATED FORMULA DUE TO BAME[43].

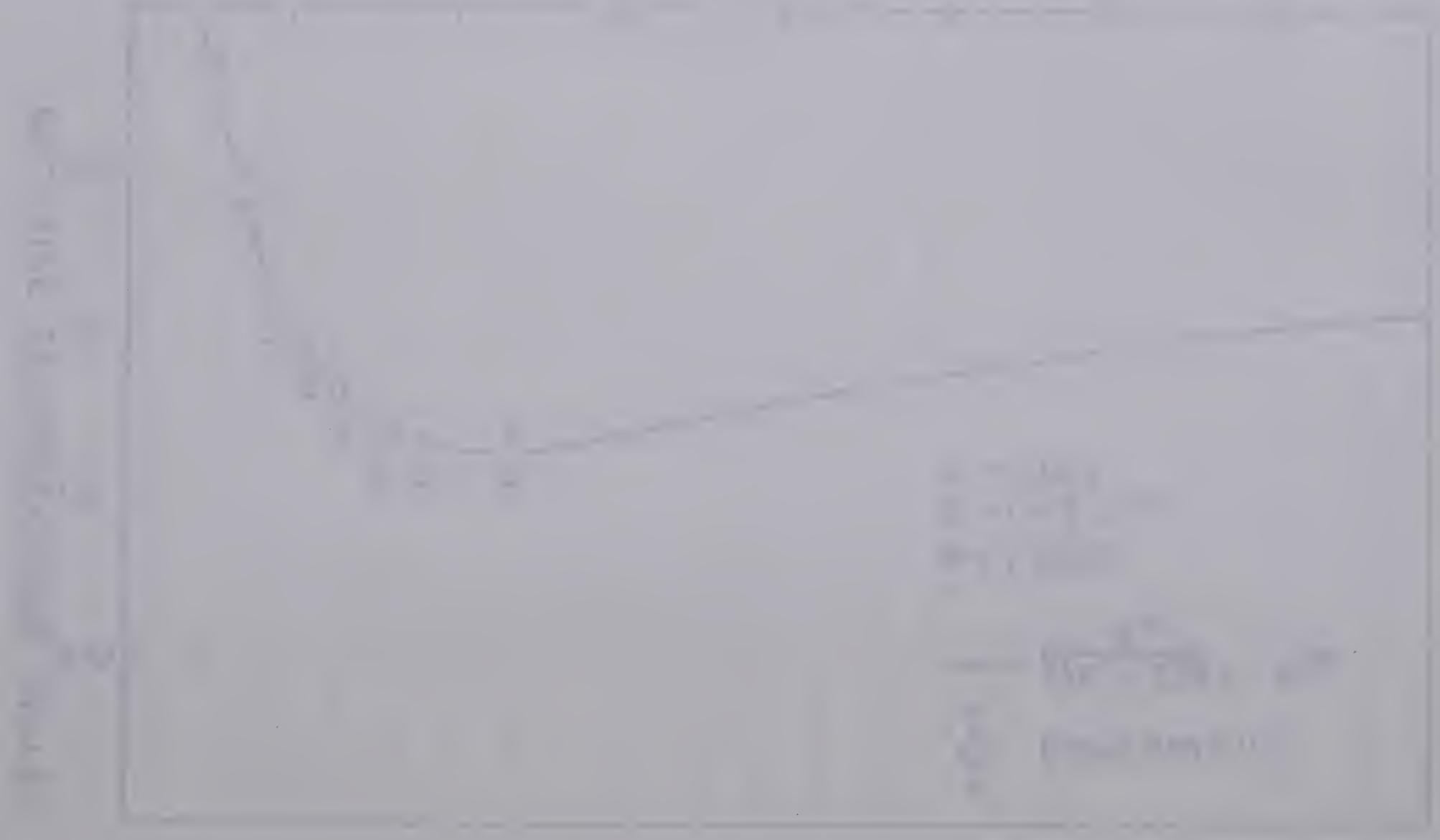

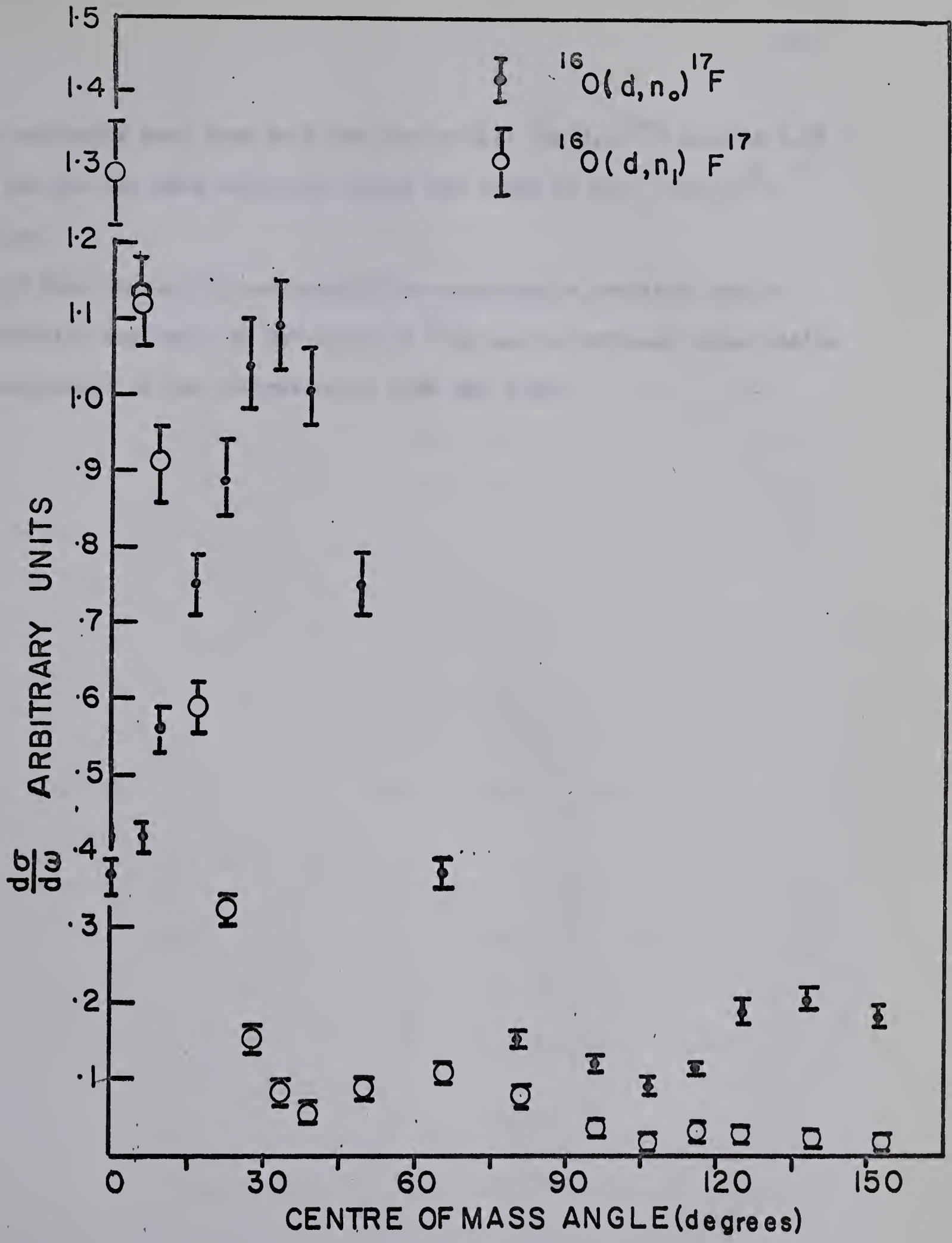

Fig.7. The relative angular distributions of the $^{16}O(d,n_o)^{17}F$, $^{16}O(d,n_1)$ reactions at E_d=5.54MeV. The relative yields are given in Appendix B on page 73.

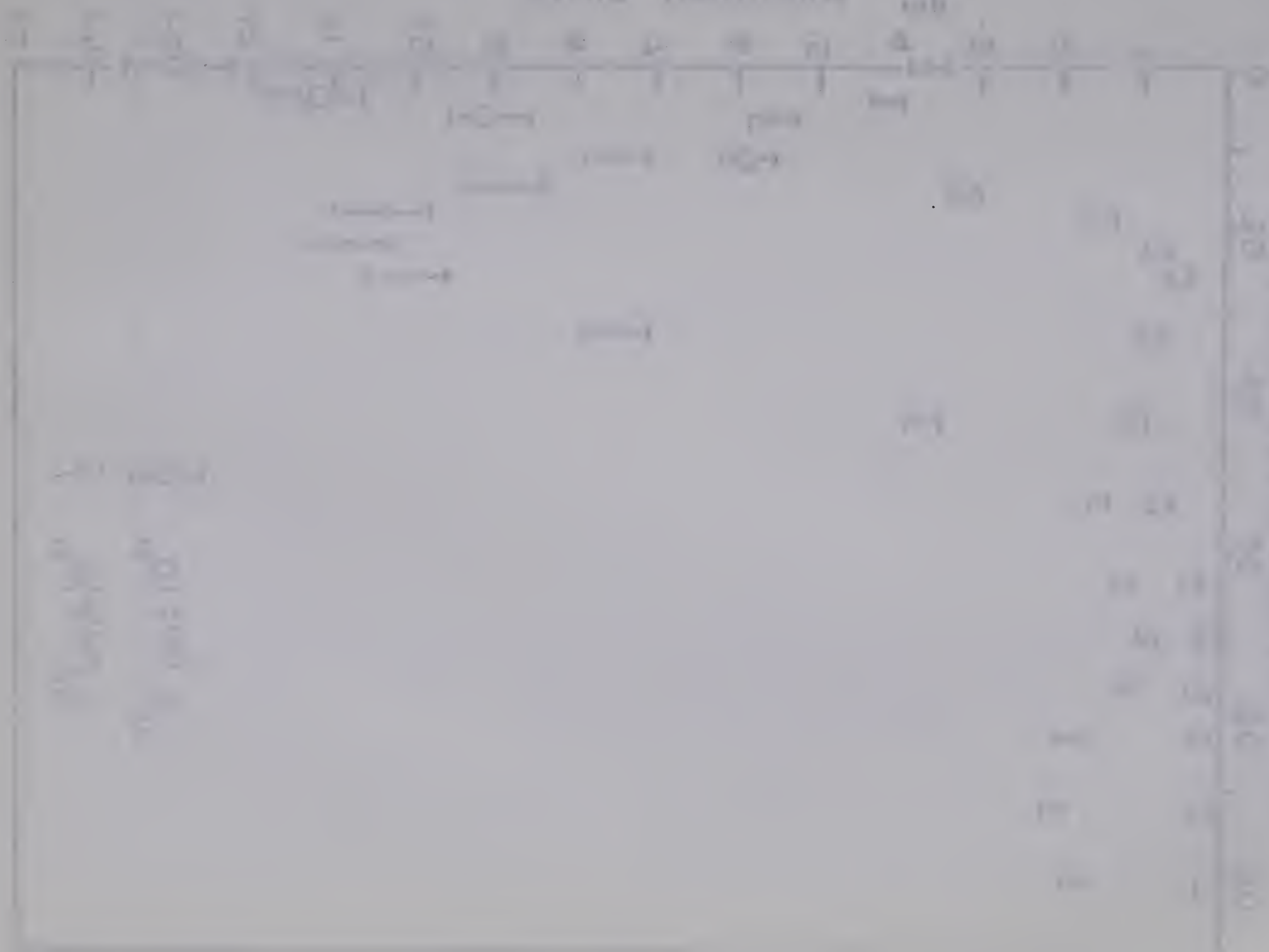

These estimates were made both for the initial $^{9}Be(d,n)^{10}B$ data at 5.54 MeV, and for the data collected during the study of the $^{16}O(d,n)^{17}F$ reaction.

In this fashion it was possible to construct a complete angular distribution for the 5.93 MeV state of ^{10}B, and to estimate upper limits for excitation of the controversial 6.40 MeV state.

CHAPTER IV. DATA INTERPRETATION

4.1 Results of Excitation Analysis for Weak States

A careful study of all the measured spectra has revealed no significant evidence for the broad level at 5.18 MeV. The spectrum in fig. 4 represents a run with the best time and energy resolution which has been achieved to date with the spectrometer used in this laboratory. Although the most modern evidence appears to confirm the existence of the 5.18 MeV level, no conclusive result can be presented here.

The effects of removing the $^{16}O(d,n)^{17}F$ contamination from the $^{9}Be(d,n)^{10}B$ spectra indicate that the peak occurring at 6.40 MeV is probably due entirely to excitation of the 0.5 MeV level of ^{17}F. The largest uncertainties of the contamination were estimated at not greater than 10% for forward angles.

This conclusion is at variance with the recent results of Bussino and Smith [15]) who report an $\ell_p = o$ angular distribution for a ^{10}B state at excitation (6.35 ± 0.05) MeV. Their DWBA fit to this neutron distribution was for angles between 0° and 35° and no account was taken of possible $^{16}O(d,n)^{17}F$ contamination.

Negative results are also reported here for the states at 5.58 MeV and 6.77 MeV. The upper limits of possible contributions due to the four weak states are presented in Table 1.

TABLE 1

The upper limits of states in ^{10}B at excitations of 5.18, 5.58, 6.40, 6.77 MeV. The 5.18 MeV limit is relative to the yield for the (5.11 + 5.16) MeV doublet. The 5.58, 6.40, 6.77 MeV limits are relative to the yield for the ^{10}B ground state. Both the areas of (5.11 + 5.16) MeV and 0.0 MeV states are set to 1.00.

Ed	3.50 MeV	5.54 MeV		
State	5.18	5.58	6.40	6.77
Angle				
0°	< 0.03	< 0.03	< 0.04	< .003
15°	< .02			
20°		< .02	< 0.04	< .005
25°			< .03	
30°	< .03	< .02	< .03	< .009
35°			< .02	
45°	< .02		< .03	< .018
60°	< .03	< .02	< .02	

4.2 Angular Distribution Interpretation

The angular distributions of fourteen neutron groups were resolved for excitations up to 7.00 MeV, and were interpreted for ℓ-values and spectroscopic factors using both the plane-wave stripping theory [44], and the DWBA code of Smith [45]. The latter makes provision for approximating the finite-range n-p interaction [28], the non-locality of nuclear forces [29], and also the deuteron polarizability [46].

The optical potentials for the deuteron and neutron channels took the following forms:

$$U(r) = -\Big(Vf(r) + iWg(r)\Big) \qquad \text{where}$$

$$f(r) = \left(1 + \exp\left(\frac{r - R}{a}\right)\right)^{-1} \qquad \text{with} \quad R = R_o A^{1/3},$$

and either $g(r) = f(r)$ (Volume absorption)

or $g(r) = 4a\,\frac{df}{dr}$ (derivative-type surface absorption).

The derivative-type form-factor is to be preferred however, since it is known that the most important contributions to stripping reactions come from the nuclear surface [64].

The interior wave function of the captured proton, F_{ℓ_p}, is calculated by starting with an asymptotic solution and then working inward numerically toward the origin. The potential well has a real Woods-Saxon part $-Vf(r)$, no imaginary part, but does include a derivative-type spin-orbit well of depth 6 MeV. The real part V is changed by trial-and-error, until the radial solution at the origin has less than

1/1000th of the value for the solution at r = Rp + 4ap.

The solutions for both the deuteron and neutron radial wave functions $F_{\ell d}$, $F_{\ell n}$, are estimated by starting with zero at the origin, 10^{-37} for r = 0.15 fm, and then working outward numerically using equation (1) (Section 1.2), until the calculated values match with prescribed asymptotic forms.

Calculations were performed both with and without a cut-off, using the zero-range and the finite-range approximations with non-local effects included.

Optical parameters for the elastic scattering of 7 MeV deuterons from ^{9}Be [47], and 14 MeV neutrons from ^{10}B [48], led to DWBA differential cross-sections in poor agreement with the 5.5 MeV data. A subsequent parameter search was undertaken for DWBA fits to the ^{10}B ground state angular distribution using the following options:

1. A zero-range calculation with Woods-Saxon form factors for the real and imaginary optical well depths (ZR).
2. A zero-range calculation with Woods-Saxon form factors for the real parts of the optical potentials and with derivative-type form factors for the imaginary parts. These calculations were repeated with radial cut-offs of 2.5 fm, 3.0 fm, 3.5 fm (ZRCO).
3. A finite-range calculation with form factors as in 2 but no cut-off (FR).
4. A finite-range calculation with form factors as in 2 but with a cut-off of 3.0 fm (FRCO).
5. A finite-range calculation with form factors as in 2, no cut-off,

but including non-local effects using a range of β = 0.85 fm for the non-locality in the three channels (FRNL).

The purpose behind the use of these options was to investigate their effects on the magnitude and shape of the DWBA differential cross-sections calculated using the same optical parameters for all the options.

Initially only option 1 was available for calculations and an extensive parameter survey yielded many parameter combinations which gave a good overall fit to the ground state angular distributions. For this survey, the radii and diffuseness parameters were fixed at the following values:

$$R_{od} = 1.80 \text{ fm} \quad : \quad R_{op} = 1.5 \text{ fm} \quad : \quad R_{on} = 1.3 \text{ fm}$$

$$a_d = 0.7 \text{ fm} = a_p \quad : \quad a_n = 0.5 \text{ fm}.$$

This large value of the deuteron radius has been used in previous calculations at 3 MeV [49]). The following search proceedure was adopted:

(a) V_n was varied alone between 40 MeV and 70 MeV in 5 MeV steps;

(b) V_d was varied alone between 45 MeV and 120 MeV in 5 MeV steps;

(c) W_n, W_d were initially held fixed at 5 MeV, 10 MeV respectively;

(d) a given fit was then improved by adjustment of V_n, V_d, W_n, W_d in 1 MeV steps.

A list of favourable sets of V_n, V_d, W_n, W_d, is indicated in table 2.

The program employed an externally controlled increment proceedure to determine optimum parameter combinations. The theoretical and experimental distributions were superposed in a logarithmic plot and a fit

TABLE 2. Potential sets yielding acceptable fits to the $^{9}B(d,n_o)^{10}B$ distribution using a zero-range DWBA calculation.

No.	$-V_n$	$-W_n$	$-V_d$	$-W_d$	(MeV)	$-V_p$ = 45MeV
1	44	6	50	9	R_{on} = 1.30fm : a_n = 0.5fm	
2	45	4	48	8		
3	55	5	79	9	R_{od} = 1.80fm: a_d = 0.7fm	
4	55	4	77	2		
5	57	4	80	8	R_{op} = 1.50fm: a_p = 0.7fm	
6	57	4	79	10		
7	57	5	78	11	for all sets listed	
8	60	5	81	8		
9	60	4	80	10	opposite.	
10	60	4	79	11		
11	62	4	82	8		
12	62	5	81	10		
13	64	4	82	9		

TABLE 3. Potential sets yielding acceptable fits to the $^{9}Be(d,n_o)^{10}B$ distribution using a finite-range DWBA calculation with non-local effects included.

No.	$-V_n$	$-W_n$	$-V_d$	$-W_n$	(MeV)	$-V_p$ = 40MeV
14	55	9.5	50	6.6	R_{on} = 1.35fm : a_n = 0.55fm	
15	50	4.0	55	10.0	R_{od} = 1.48fm : a_d = 0.63fm	
16	55	6.0	62	10.0	R_{op} = 1.48fm : a_p = 0.63fm	
					for all sets listed opposite.	

was tested visually. A value of chi-squared was calculated for each pair of distributions and this also gave a measure of the goodness-of-fit.

When options 2, 3, 4, 5 became available with the Smith code, a parameter search was undertaken using option 5. For this case the radii and diffuseness parameters were fixed at the following values:

$R_{od} = 1.48$ fm : $R_{op} = 1.48$ fm : $R_{on} = 1.35$ fm [47])

$a_d = 0.63$ fm : $a_p = 0.63$ fm : $a_n = 0.55$ fm [48])

Initially the values of W_n, W_d were held fixed at 9.5 MeV and 6.6 MeV respectively. (These values were also taken from refs. 47, 48).

The search proceedure of option 1 was then carried out. With this survey, fewer parameter sets were found which gave the quality of the fits obtained with option 1. None of the sets of table 2 gave a good overall fit for the ground state distribution although the main stripping peak was generally reproduced. Some of best-fit sets determined from this survey are listed in table 3.

Using the potential sets of tables 2 and 3 with the appropriate options, DWBA cross-sections were generated for all the resolved neutron distributions corresponding to bound ^{10}B levels. States in ^{10}B with Q-values of less than -2.226 MeV became unbound to proton emission, and the DWBA code used was unable to describe stripping to virtual levels. (There is a DWBA theory for such stripping [50]) but it has been used in only one published case to date [51])). As a point of interest, computational difficulties arose with the Smith code for Q-values less

than -2.00 MeV. This was found to be due to the numerical range allowed by the IBM 7040 computer which performed the calculations.

The angular distributions which could not be described, corresponded to ^{10}B excitations at 6.57 MeV (Q = -2.21 MeV), 6.88 MeV (Q = -2.52 MeV), and 7.00 MeV (Q = -2.64 MeV).

Satchler [52]) and Smith [53]) have both advised that the Q-values for these states be adjusted until a bound condition is obtained (Q $\doteqdot$ -2.00 MeV). One can argue heuristically that provided the "captured" proton remains significantly below the Coulomb plus centrifugal barrier, its wave function looks presumably much like a bound state save for a slow decay. Other than seeming reasonable, there is no physical justification of this proceedure.

Regarding the DWBA fits, it was found that a parameter set yielding a good overall fit for the ground state distribution, generally did not accurately describe the excited state distributions away from the main stripping peak. Single parameter sets however resulted in unambiguous ℓ-values for the following states (MeV):

0.0, 0.72, 1.74, 2.15, 5.11, 5.16, 5.93, 6.14.

These ℓ-values were confirmed by plane-wave calculations performed concurrently using a "stripping" radius of 5 fm for all the calculations.

The results of DWBA calculations for ten bound states are presented in figs. 8, 9, and 10, using the single parameter set listed in fig. 8. Superposed for each state are the curves resulting from options 2, 3, 5. The plane-wave calculations for the states at 6.57, 6.88, 7.00 MeV are

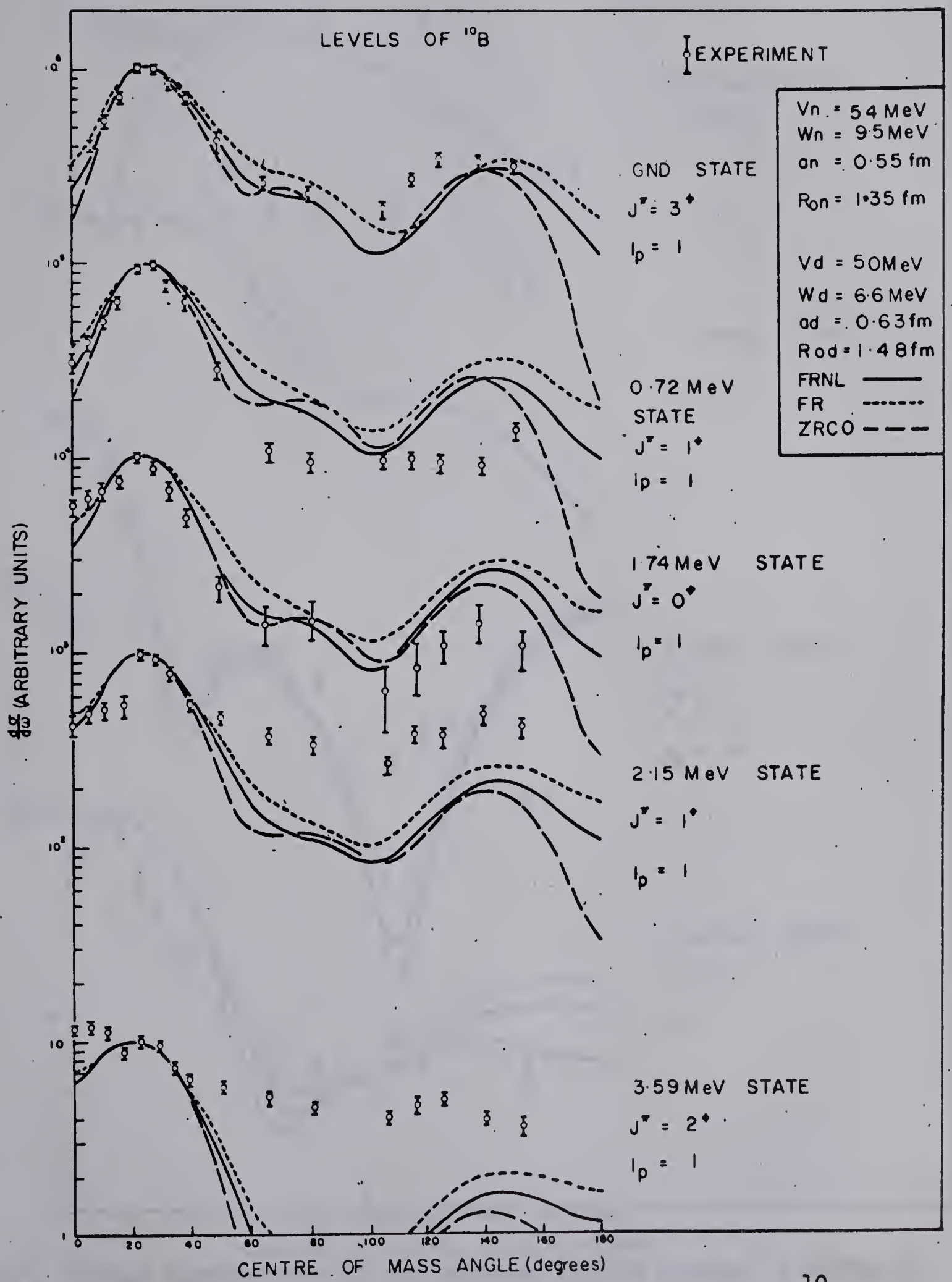

FIG.8. ANGULAR DISTRIBUTIONS OF THE NEUTRONS LEADING TO THE ^{10}B STATES AT 0.0, 0.72, 1.74, 2.15, AND 3.59 MeV FOR E_d = 5.54 MeV. THE SMOOTH CURVES ARE DWBA CALCULATIONS WITH THE PARAMETERS LISTED, USING THE OPTIONS DESCRIBED IN THE TEXT.

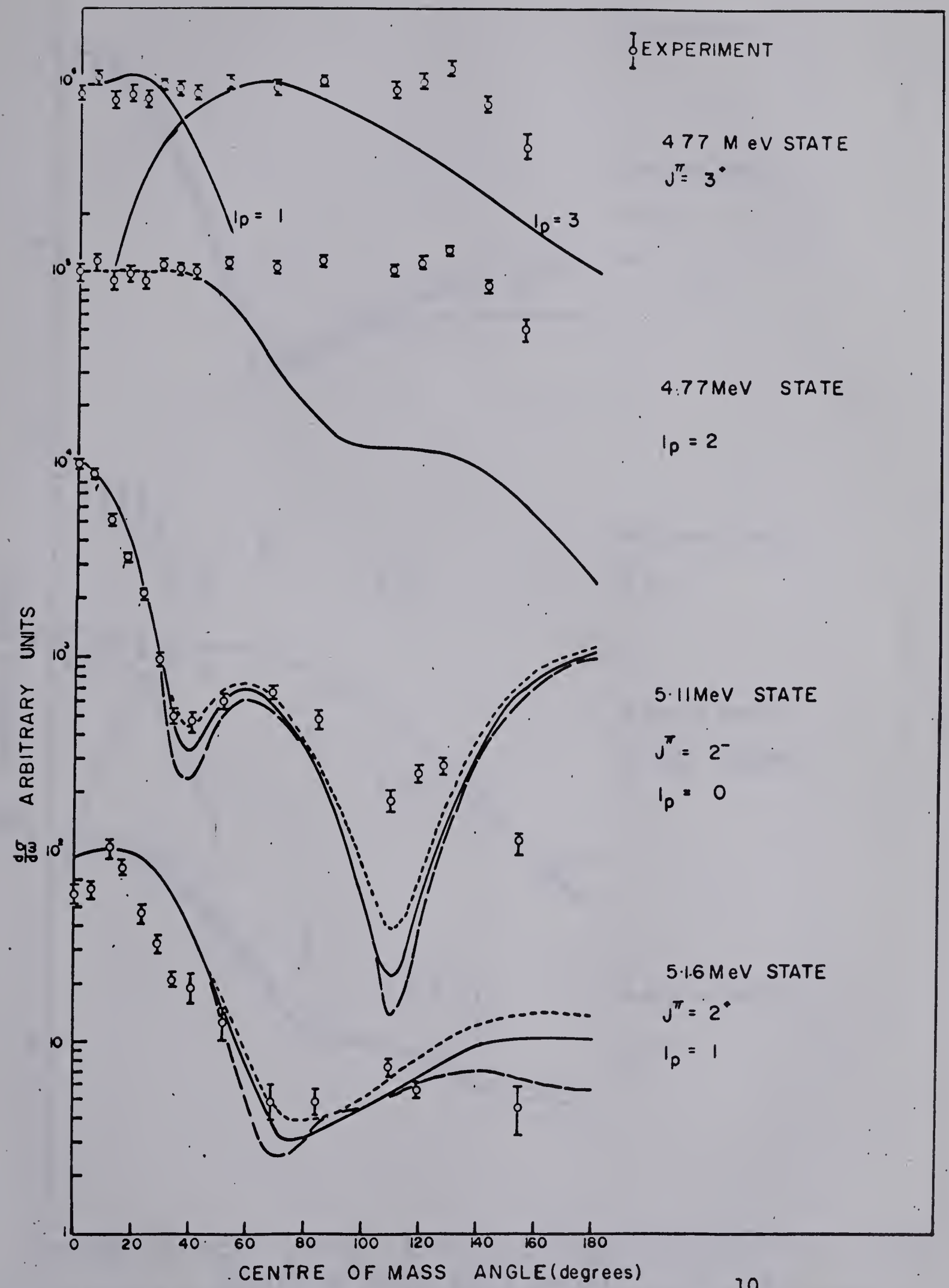

FIG.9. ANGULAR DISTRIBUTIONS OF THE NEUTRONS LEADING TO THE ^{10}B STATES AT 4.77, 5.11, 5.16 MeV FOR E_d = 5.54 MeV. THE SMOOTH CURVES ARE DWBA CALCULATIONS USING THE PARAMETERS AND OPTIONS LISTED ON FIG.8.

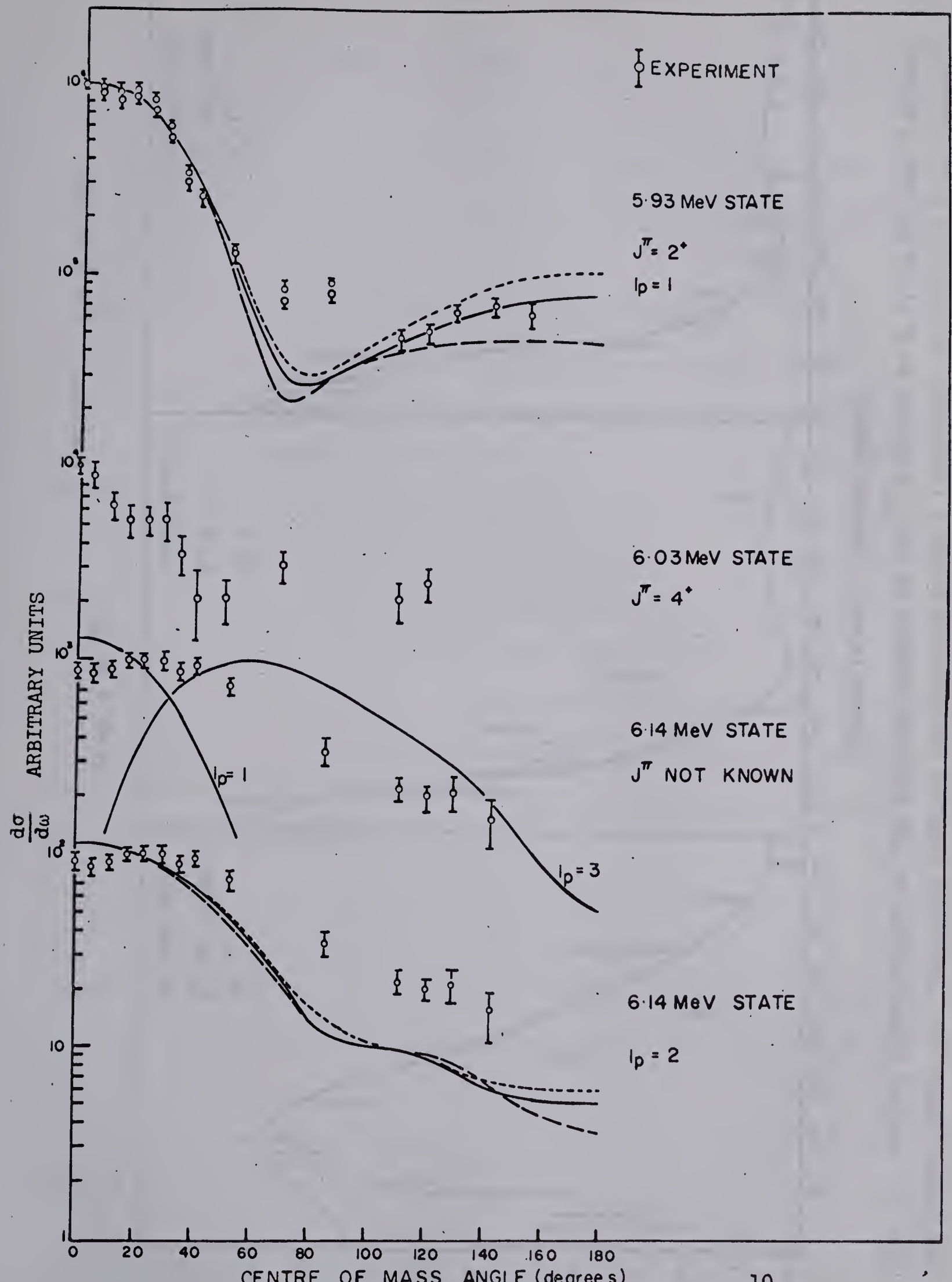

FIG. 10. ANGULAR DISTRIBUTIONS OF THE NEUTRONS LEADING TO THE ^{10}B STATES AT 5.93, 6.03, 6.14 MeV, FOR E_d = 5.54 MeV. THE SMOOTH CURVES ARE DWBA CALCULATIONS USING THE PARAMETERS AND OPTIONS LISTED ON FIG.8.

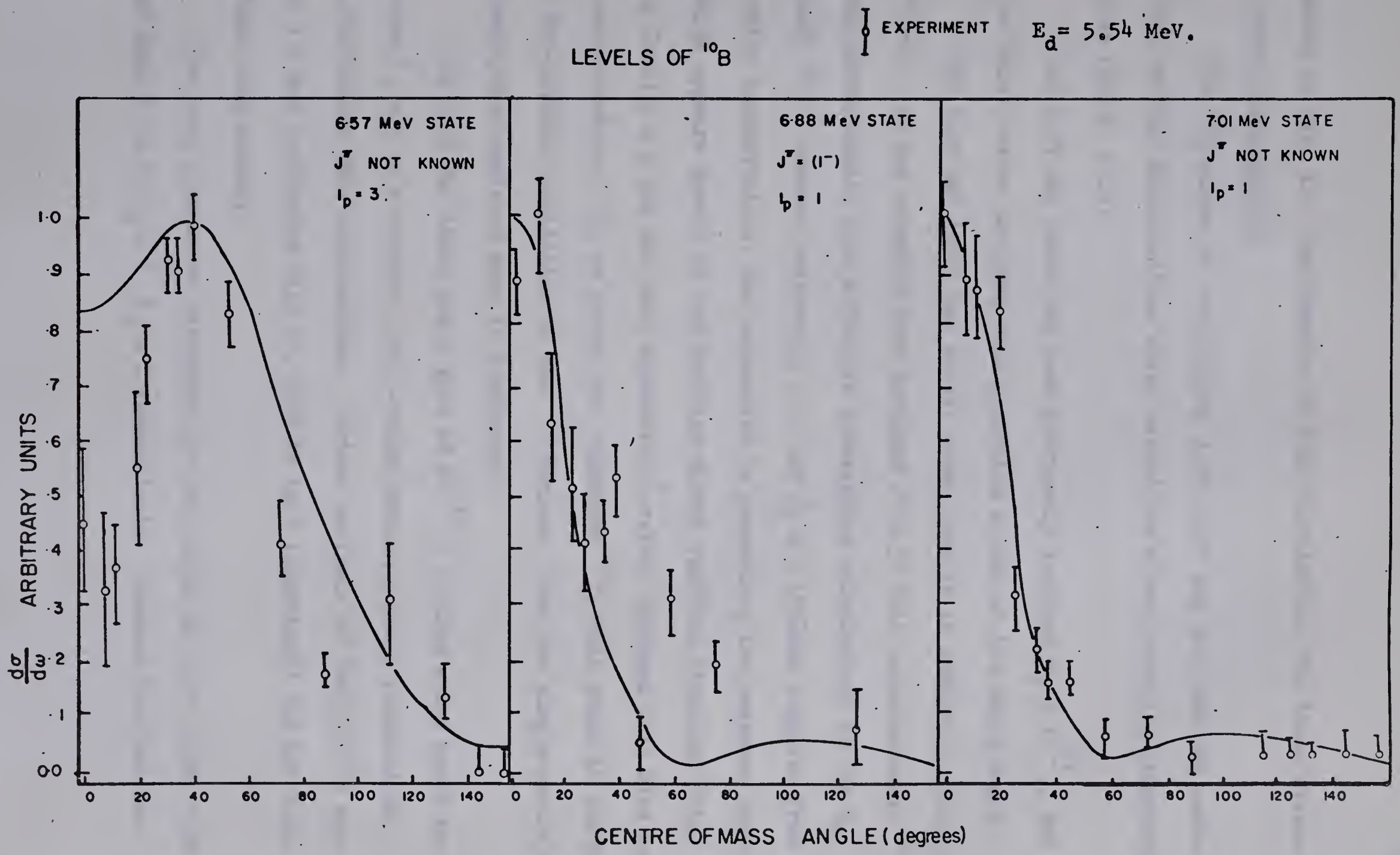

FIG. 11. ANGULAR DISTRIBUTIONS OF THE NEUTRONS LEADING TO THE ^{10}B STATES AT 6.57, 6.88, AND 7.01 MEV. THE SMOOTH CURVES ARE PLANE-WAVE (BUTLER) CALCULATIONS USING A 'STRIPPING' RADIUS OF 5.0 FM THROUGHOUT.

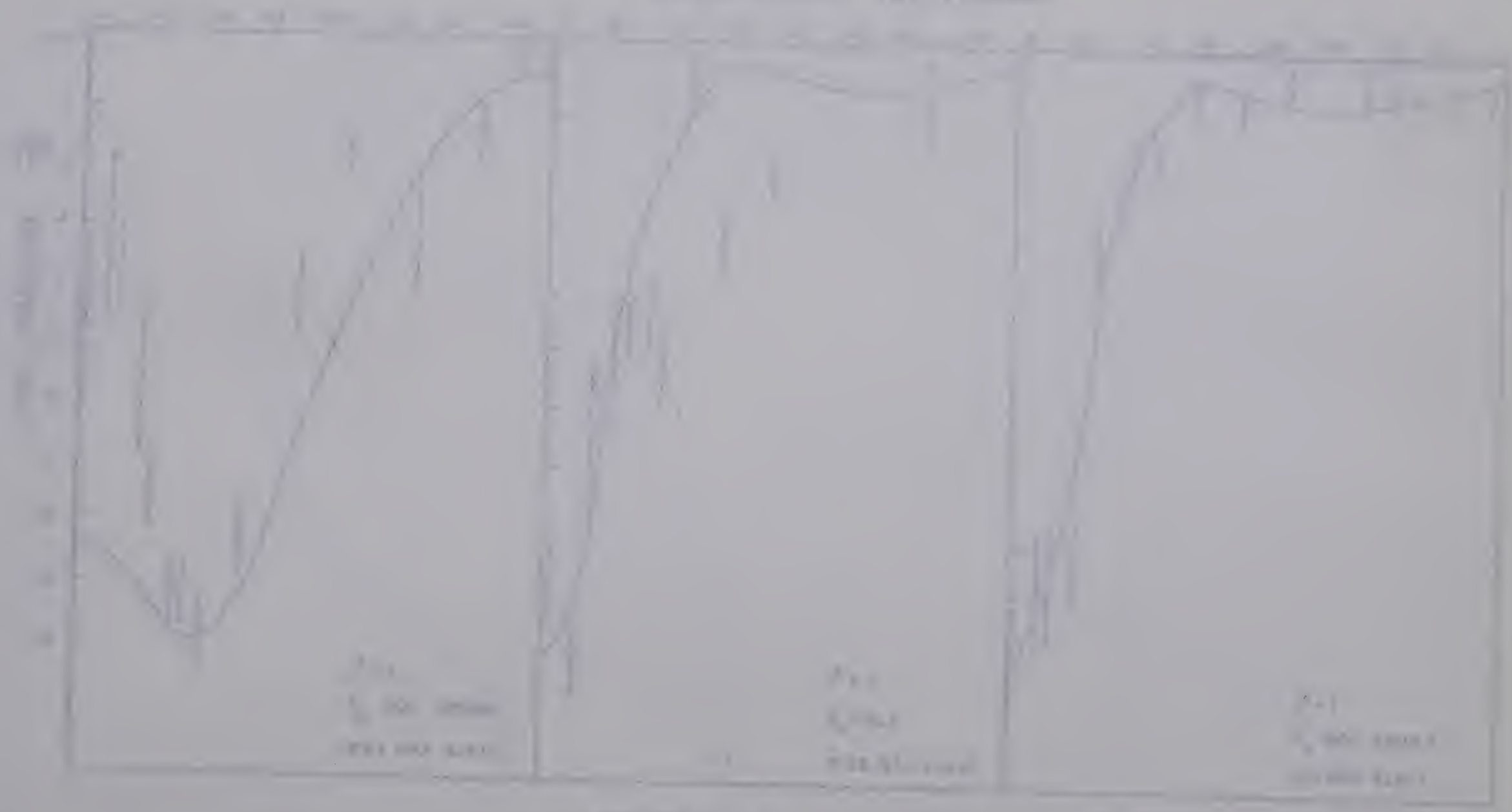

shown in fig. 11. The results of DWBA calculations for these states proved unsuccessful.

The ^{10}B states at excitations 3.59, 4.77 and 6.03 MeV had anomalous neutron distributions which defied the direct reaction interpretation (figs. 8-10)

The 3.59 MeV level has been previously assigned $\ell_p = 1$ [15]), but for this ℓ-value the DWBA code generated a peak at the wrong angle.

The 4.77 MeV level has always given trouble in stripping reactions [14,15]). It has recently been assigned $J^\pi = 3^+$ both experimentally [54]), and theoretically from effective interaction calculations in the 1_p shell [55]). However neither $\ell_p = 1$, nor $\ell_p = 3$ (values required from parity conservation), was successful in generating the measured shape, which appears devoid of the familiar direct reaction structure (fig. 8). In fact $\ell_p = 2$ was the most successful ℓ-value, although this also was unsatisfactory. If, as Kurath has suggested [15]), this state is due to a two-particle excitation of the ^{10}B nucleus, then the single-particle description employed here is inadequate.

The 6.03 MeV level has a spin of 4^+ [10]), a value which would require $\ell_p = 3$ as a minimum. No ℓ-value between 0 and 3 resulted in satisfactory DWBA calculations. Further analysis of $^9Be(d,n)^{10}B$ data at 3.5 MeV (collected July 17, 1964 in this laboratory) did not eliminate this anomaly.

The best plane-wave estimates for the states at 6.57, 6.88, 7.00 MeV gave $\ell_p = 3$, $\ell_p = 1$, $\ell_p = 1$ respectively. However the last two

TABLE 4. MEASURED STATES OF ^{10}B

This Experiment		Previous Work*			
Ex (MeV ± keV)	ℓ_p	ℓ_p	Ex (meV ± keV)	J^π	T
0.0	1	1	0.0	3^+	0
0.72 ± 10	1	1	0.7173 ± 0.8	1^+	0
1.74 ± 10	1	1	1.740 ± 2	0^+	1
2.15 ± 10	1	1	2.154 ± 3	1^+	0
3.58 ± 10	(1)	1	3.585 ± 4	2^+	0
4.77 ± 10	(2,3)	≥ 2 [15]	4.774 ± 3	3^+ [35]	0
5.11 ± 12	0	0	5.114 ± 4	(2^-)	0
5.17 ± 14	1	1	5.166 ± 4	2^+	1
			5.183 ± 8 [6,8]	1^+	0
			5.58		
5.93 ± 10	1	1	5.923	2^+	0
6.03 ± 12			6.029 ± 4	4^+	
6.14 ± 10	(2)	(2)	6.133 ± 4		
		(0)	6.35 ± 50 [15]		
6.57 ± 10	(3)	1	6.566 ± 6		
			6.77 [6]		
6.89 ± 15	(1)		6.884	1^-	0
7.00 ± 12	(1)		7.00		
			7.431 ± 10	2^-	0
			(7.468 ± 10)	(2^+)	
7.48 ± 15			7.479 ± 2	(2^-)	
7.56 ± 25			7.561 ± 1	0^+	1

*All information taken from ref. [68] unless otherwise marked.

| | | |

ℓ-values must be adopted with caution because of probable contamination of the neutron distributions from $^{12}C(d,n_1)^{13}N$ reaction.

The ℓ-values from this set of experiments, together with the mean ^{10}B excitations and errors, estimated with the least-squares code, are compared with previous measurements in table 4.

The fact that a ground state best-fit set of parameters did not yield a good overall fit for the excited state distributions, prompted an investigation of the effects of varying the values of V_n and W_n for the excited states. Generally a given fit could be improved by adjusting V_n and W_n alone. However, there did not appear to be any systematic correlation of the neutron parameters with excitation energy. Siemssen et al [49]) have suggested that the optical parameters for such a light nucleus might depend on the configuration of the outer nucleons which presumably varies from state to state.

However, considering the uncertainties of compound nucleus contributions, and the inadequacies of the stripping formulation for this mass number and bombarding energy, it is hardly surprising that one set of parameters does not completely describe the excited state distributions.

On the basis of calculations performed on the relative angular distribution alone, it is difficult to compare the merits of options 1 to 5. For a given potential set with the same radial form factors, only small changes in the calculated angular shapes are detectable. Presumably option 5, with finite-range and non-local effects included

represents the most accurate calculation.

The use of a radial cut-off, advocated by Satchler [56]) to eliminate erroneous contributions from the nuclear interior is a most drastic solution although it appears to improve a zero-range fit for back angles.

From an extensive series of calculations performed on the $^{40}Ca(d,p)^{41}Ca$ reaction [57]), it is known that the inclusion of finite-range and non-local effects tends to dampen contributions from the nuclear interior, thus reducing the need for a cut-off. However, the non-local correction tends to enhance the tail of the bound state wave function, so that although interior contributions are diminished, the cross-section magnitude is unchanged from calculations performed without a cut-off.

As an illustration of these effects, the different deuteron radial wave functions for the ground state transition, calculated using options 3, 5 are indicated in fig. 12.

In their study of the $^{40}Ca(d,p)^{41}Ca$ reaction from 7.00 MeV to 12.00 MeV deuteron energy, Lee et al [57]) came to the conclusion that the best agreement with experiment could be achieved by using a deuteron potential of real depth 120 MeV, roughly twice the nucleon potential. Recently, Greider and Strobel [58]) have advocated using a deuteron potential equal to the sum of the neutron and proton potentials. For nuclei where $\langle r_{np} \rangle << R_{nucleus}$, they indicate how such a deuteron potential more accurately justified the use of V_{np} as the

residual interaction in stripping.

Although Greider and Strobel's conditions are not met with in the $^{9}Be(d,n)^{10}B$ reaction, some finite-range DWBA calculations were performed for deuteron potentials between 80 MeV to 140 MeV (V_d) A tolerable fit to the ground state distribution was obtained using the FRNL option for a deuteron potential of about 110 MeV. However this aspect of the calculations was not pursued in any detail and no calculations for the excited states were made.

4.3 Calculation of Spectroscopic Factors

In the case where only one ℓ-value and j-value are important in a stripping transition, the spectroscopic factor can be defined by the normalisation

$$\left(\sigma(\theta)\right)_{exp} = S_\ell \cdot \left(\sigma_{\ell j}(\theta)\right)_{DWBA}$$

However for only three of the measured states---0.0, 1.74, 5.11 MeV--- were the j-values known explicitly (j = 3/2, 3/2, 1/2 respectively). For the others, $j = \ell + 1/2$, or $j = \ell - 1/2$, were allowed. Since the bound proton has a spin-orbit well of depth 6.00 MeV, the ambiguity in j will be reflected in uncertainty in the absolute DWBA cross-sections, and hence in the spectroscopic factors. For the states where uncertainty in j existed, calculations were performed with both j-values, and this led to DWBA cross-sections for a given state differing by a maximum of 7%. All the spectroscopic factors reported here have $j = \ell + 1/2$. Since relative cross-sections only were measured the spectroscopic factors have been normalised to a ground state value of

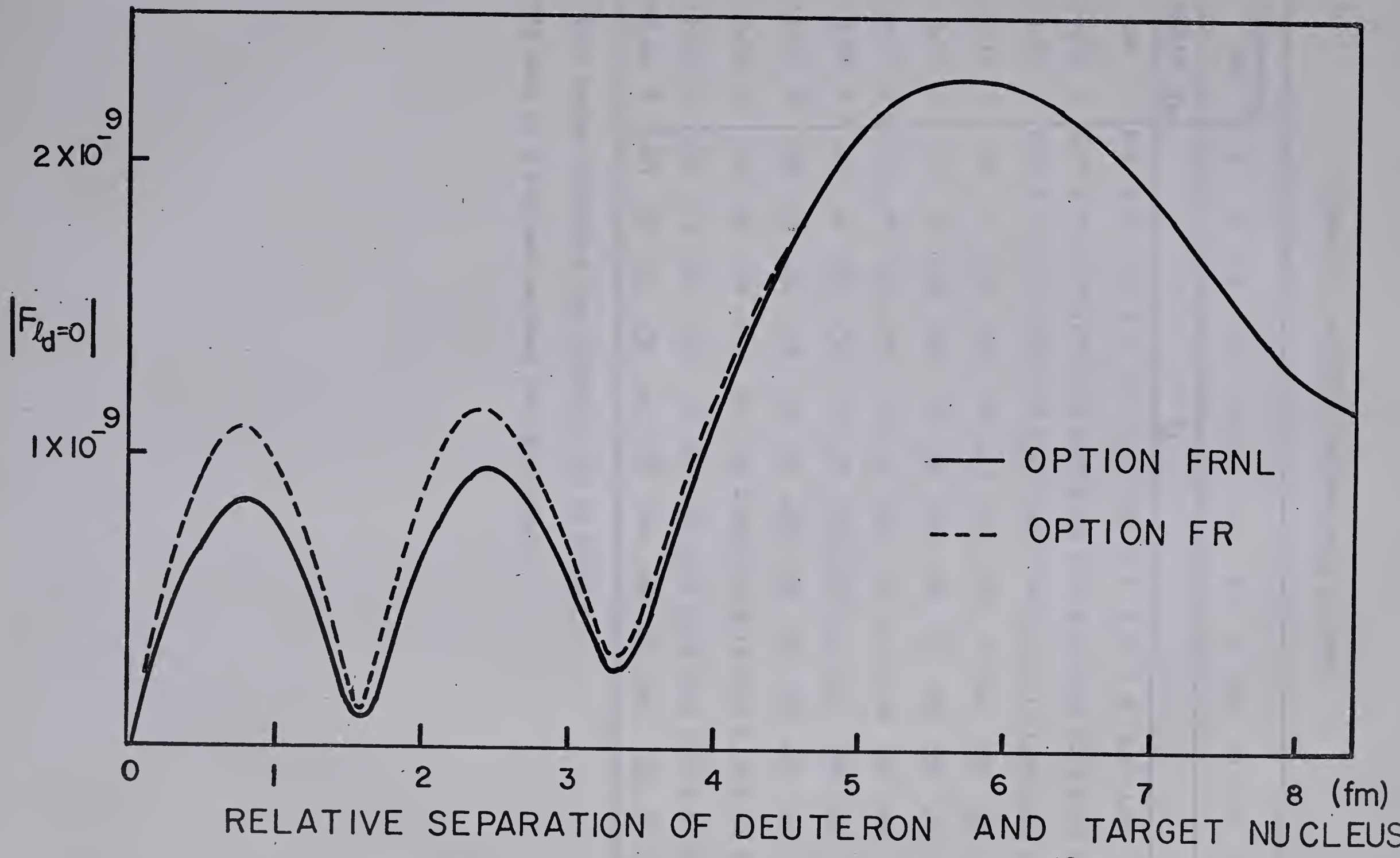

FIG.12. RADIAL DEUTERON WAVEFUNCTIONS FOR THE $^{9}BE(d,n_0)^{10}B$ TRANSITION USING THE OPTICAL PARAMETERS LISTED ON FIG.8. THE OPTIONS REFER TO CALCULATIONS WITH (FRNL) AND WITHOUT (FR) THE NON-LOCAL FORM FACTOR. NON-LOCAL EFFECTS REDUCE $|F_{\ell_d}|$ BY ABOUT 25% INSIDE THE NUCLEUS (<3 fm).

TABLE 5. RELATIVE SPECTROSCOPIC FACTORS

*Potential Set		1	2	3	4	5	6	7	8	9	10	11	12	13
State	ℓ_p	S_ℓ												
Gnd	1	1.0	1.0	1.0	1.0	1.0	1.0	1.0	1.0	1.0	1.0	1.0	1.0	1.0
0.72	1	2.76	2.79	2.79	2.77	2.78	2.75	2.75	2.73	2.72	2.75	2.69	2.70	2.65
1.74	1	1.83	1.79	1.74	1.82	1.82	1.91	1.97	2.04	2.13	2.18	1.95	1.84	1.99
2.15	1	.78	.71	.66	.69	.64	.63	.63	.60	.58	.61	.59	.59	.58
3.59	1	.43	.37	.67	.64	.72	.67	.66	.70	.65	.60	.67	.63	.64
4.77	1	.56	.48	.55	.44	.62	.58	.56	.65	.58	.54	.45	.48	.45
4.77	2	.45	.40	.29	.36	.64	.79	.72	1.08	1.06	1.07	.84	.88	.80
5.11	0	.59	.54	.51	.58	.54	.61	.66	.46	.53	.58	.41	.46	.45
5.16	1	.55	.62	.74	.75	.82	.99	1.00	1.16	1.18	1.17	1.12	1.12	1.07
5.93	1	.81	.73	.69	.63	.74	.79	.81	1.10	1.13	1.17	1.18	1.05	1.17
**6.14	2	.83	.26	.36	.32	.43	.47	.44	.60	.65	.61	.53	.69	.63

*The number indicates the potential set in Table 2.

**A spin of 3 has been assumed for this level.

TABLE 6. Relative spectroscopic factors for all ^{10}B states up to 6.14 MeV excitation, using the potential sets listed in TABLE 3.

Potential No.		14	14	14	14	15	16
Option		ZRCO	FRCO	FR	FRNL	FRNL	FRNL
STATE	ℓ_p	S_ℓ					
Gnd.	1	1.0	1.0	1.0	1.0	1.0	1.0
0.72	1	2.98	2.96	2.93	2.65	2.68	2.72
1.74	1	1.45	1.44	1.54	1.44	1.61	1.48
2.15	1	0.46	0.46	0.51	0.49	0.56	0.53
3.59	1	0.24	0.24	0.28	0.27	0.33	0.29
4.77	1	0.07	0.07	0.09	0.08	0.11	0.09
4.77	2	0.36	0.38	0.42	0.44	0.33	0.39
5.11	0	0.39	0.50	0.70	0.62	0.63	0.55
5.16	1	0.49	0.49	0.61	0.59	0.65	0.54
5.93	1	0.59	0.59	0.78	0.75	0.73	0.67
*6.14	2	0.50	0.50	0.72	0.63	0.58	0.55

* A spin of 3 has been assumed for this state when calculating the spectroscopic factors.

TABLE 7. Comparison of measured relative spectroscopic factors with previous experimental and theoretical values.

		Spectroscopic Factors				
STATE	ℓ_p	Plane wave values	Average DWBA values	Previous DWBA values[15])	Theoretical[61]) S(lp)2B	S(lp)Pot*
Gnd	1	1.0	1.0	1.0	1.0	1.0
0.72	1	2.75	2.77±.10	2.30	1.38	
1.74	1	1.27	1.78±.20	1.00	1.96	
2.15	1	0.61	0.60±.11	0.41	0.42	
3.59	1	0.29	0.51±.20	0.45	0.09	0.32
4.77	1	0.06			0.02	0.01
4.77	2	0.40	0.68±.30	0.43		
5.11	0	1.66	0.54±.13	1.30		
5.16	1	0.47	0.82±.25		0.16	0.23
5.93	1	0.66	0.84±.15		0.54	0.35
6.14	2	0.30	0.52±.22			

* The spectroscopic factor for a lp nucleon is the number of lp nucleons in ^{10}B times the squares of the coefficients of fractional parentage for the ^{10}B states in question, summed over the $lp^{3/2}$ and $lp^{1/2}$ components. Kurath has done this for two lp-shell residual interactions - the (8-16)Pot and the (6-16)2B described in ref. [55]). For both interactions, the ground state of ^{10}B has an absolute theoretical spectroscopic factor of 1.2.

1.0.

Relative factors were calculated for all the potential sets of tables 2 and 3 and for all the calculations of figs. 8 to 10. The plane-wave values were also determined using the semi-empirical methods of French [59]). The factors calculated for all excited states of ^{10}B up to 6.14 MeV are indicated in tables 5, 6, and 7.

The first point to note is the similarity between the plane-wave values, and many of the DWBA sets. Although the absolute spectroscopic factors would bear no relation, the relative values appear to be comparatively stable, and all the sets calculated show the same general trends with excitation energy.

The absolute DWBA cross-sections at the peak angles for options 2 to 5 where the same potential set was employed, are listed in table 8. Using a cut-off of 3 fm in the zero-range approximation would appear to reduce the absolute cross-sections by a factor of about 2.5 from the finite-range non-local values. However the spectroscopic factors for these two options are very similar, differing by no more than 15% in most cases.

Also in all cases, the inclusion of non-local effects tends to slightly increase the cross-section over the values determined with the finite-range approximation alone. This increase occurs despite the fact that contributions from the nuclear interior are damped, and as already mentioned, is due to the non-local enhancement of the bound state tail.

TABLE 8. ABSOLUTE DWBA CROSS-SECTIONS (mb/sr) at $\theta_{max.}$*

State	ℓ	ZRCO	FRCO	FR	FRNL
Gnd	1	7.45	12.30	17.60	17.71
0.72	1	3.25	5.40	7.80	8.60
1.74	1	1.48	2.45	3.30	3.50
2.15	1	5.05	8.36	11.00	11.20
3.58	1	12.00	19.70	24.30	25.0
4.77	1	22.40	36.8	43.00	44.50
4.77	2	4.70	6.30	9.60	9.70
5.11	0	10.60	13.70	13.90	15.60
5.16	1	18.40	30.10	34.70	35.70
5.93	1	23.40	38.20	42.3	43.80
6.14	2	6.77	11.0	11.2	12.60

*Calculations performed using only the set of parameters in fig. 8.

The average DWBA values with errors are compared in table 7 with

1. plane-wave estimates
2. previous measurements of Bussino and Smith [15])
3. theoretical values calculated by Kurath [60]).

The errors were estimated from the spread of the calculated values. An additional 10% error is introduced from uncertainties in the relative yields to the various states.

The agreement with theory is poor, especially for the 0.72 MeV state, and in general the average values do not closely agree with the previous measurements. For some states e.g. 0.72, 2.15 there is very close agreement between the averaged and the plane-wave factors, while other pairs differ by almost a factor of 2.

4.4 Conclusions

The search for the four weak states of ^{10}B has resulted in negative evidence for all of them. When considered in the light of previous measurements using this and other reactions, it is felt that the ^{10}B levels at 5.58, 6.40, 6.77 MeV are spurious. Although the 5.18 MeV level was not detected in this reaction, published evidence would appear to support its existence. The presence of a level at this excitation neatly explains the decay of the 7.56 MeV level of ^{10}B [1]). Also, one cannot discard the results from the $^{10}B(d,d')^{10}B^*$ reaction [4]). The fact that no significant trace has been found would indicate that the strong 5.11 - 5.16 MeV doublet almost completely masks whatever weak excitation is present.

From the DWBA study of the $^{9}Be(d,n)^{10}B$ reaction at 5.5 MeV several points emerge. The first point is that in any stripping reaction it is of crucial importance to determine the optical parameters to be later used in the DWBA analysis. These parameters should be preferably determined using the target to be employed in the stripping reaction study. (In this way, isotopic or other differences should not affect the parameters.)

This foreknowledge will avoid the somewhat arbitrary search proceedure carried out in this report. In previous cases where parameters were first measured (e.g. ref. [57]), a reasonable degree of success was achieved. Even for this classic case however, several parameter sets yielded impeccable fits to the scattering data. Unfortunately these sets resulted in differing absolute DWBA cross-sections and hence differing spectroscopic factors. This was also the case in the calculations of W.R. Smith [61]) who concluded that spectroscopic factors are not accurately determined using the present DWBA formalism. Despite these difficulties, prior knowledge of the parameters is by far the best approach to DWBA calculations.

The remarks of Schiffer *et al* [62]) are also highly relevant. They point out that with present day developments in the optical model, it is not sufficient to measure optical parameters for one nucleus at one bombarding energy. Rather one should measure energy- and mass-averaged parameters over a range of intermediate energies, with masses in the region of the nucleus under study.

The second point of interest concerns the sensitivity of the calculated cross-sections (and hence spectroscopic factors) to optical parameter uncertainties and the precise mode of calculation. The cross-sections listed in table 8. for a single parameter set illustrate how drastically cross-sections can change with the different options. In a sense, there are too many prescriptions for doing DWBA calculations. With regard to this point Pinkston and Satchler [63]) have indicated how critically the calculations depend on the wave function used for the captured particle. In carrying out a search for DWBA fits to stripping data as in this report, it would appear best to confine the calculations to the FRNL option. This represents the most sophisticated calculation and simulates the effects of using a radial cut-off, by dampening contributions from the nuclear interior.

The efforts to reproduce the measured angular distributions with one set of optical parameters has met with only partial success. Generally the main stripping peak is reproduced for the excited states when using one set, but there is poor agreement with the cross-sections at large angles. This may be due to compound nucleus effects which will be proportionately more important at these angles.

In conclusion, the calculations appear to show that at this energy, many of the observed transitions in the $^{9}Be(d,n)^{10}B$ reaction appear to be due to a direct reaction mechanism although the DWBA theory as formulated may not be an accurate description.

BIBLIOGRAPHY

In the following list, DINRM refers to "Direct Interactions and Nuclear Reaction Mechanisms" edited by E. Clementel and G. Villi (Gordon and Breach New York, 1963).

1 E.C. Sprenkel, J.W. Olness, R.E. Segel, Phys. Rev. Lett. 7 (1961) 174.

2 G. Dearnaley D.S. Gemmell, S.S. Hanna, Nucl. Phys. 36 (1962) 71.

3 R.E. Meads, J.E.G. McIldowie, Nucl. Phys. 33 (1962) 502.

4 B.H. Armitage, R.E. Meads, Phys. Lett. 1 (1962) 284.

5 A.T.G. Ferguson, N. Gale, G.C. Morrison, R.E. White, in DINRM p. 510.

6 F. Ajzenberg, Phys. Rev. 88 (1952) 298.

7 E. Hjalmar, H. Slätis, Arkiv för Fysik 18 (1960) 193.

8 J.J. Singh, Phys. Rev. 114 (1959) 871.

9 T. Bonner, C. Cook, Phys. Rev. 96 (1954) 122.

10 L. Meyer-Schützmeister, S.S. Hanna, Phys. Rev. 108 (1957) 1506.

11 J. Bourotte, J. Phys. Rad. 22 (1959) 583.

12 B.H. Armitage, R.E. Meads, Phys. Lett. 8 (1964) 346.

13 S. Gorodetsky, A. Gallmann, R. Rebmeister, Phys. Rev. 137 (1965) B1466.

14 F.C. Young, P.D. Forsyth, A.R. Knudson, B.A.P.S. 10 (1965) 439.

15 S.G. Bussino, A.B. Smith, Phys. Lett. 19 (1965) 234.

16 W.F. Hornyak, C.A. Ludermann, M.L. Roush, Nucl. Phys. 50 (1963) 424.

17 M.A. Crosby, J.C. Legg, G. Roy, B.A.P.S. 10 (1965) 439.

18 M.K.Mehta, W.E. Hunt, H.S. Plendl, R.H. Davis, Nucl. Phys. 48 (1963) 90.

19 A. Gallmann, D.E. Alburger, D.H. Wilkinson, F. Hibou, Phys. Rev. 129 (1963) 1765.

20 M.L. Roush, P. Forsyth, F.C. Young, W.F. Hornyak, J.B. Marion, B.A.P.S. 10 (1965) 9.

21 P.P. Singh, D.S. Gemmell, B.A.P.S. 10 (1965) 538.

22 S.T. Butler, Proc. Phys. Soc. (London) A208 (1951) 559.

S.T. Butler, O. Hittmair, Nuclear Stripping Reactions (Wiley 1957).

23 W. Tobocman, Theory of Direct Nuclear Reactions (Oxford University Press, 1961).

24 N.K. Glendenning, Ann. Rev. of Nucl. Sci. 13 (1963) 191.

25 N. Austern, in Selected Topics in Nuclear Theory, edited by F. Janouch (International Atomic Energy Agency, 1963) p.7.

G.R. Satchler, Nucl. Phys. 55 (1964) 1.

R.H. Bassel, "Some applications of DWBA for direct nuclear reactions", Oak Ridge National Laboratory Report, ORNL-P-144 (1964).

26 S.K. Penny, G.R. Satchler, Nucl. Phys. 53 (1964) 145.

27 F.G. Perey, D. Saxon, Phys. Lett. 10 (1964) 107.

28 J.H. Dickens, R.M. Drisko, F.G. Perey, G.R. Satchler, Phys. Lett. 15 (1965) 337.

29 F.G. Perey in DINRM p. 125.

30 G.C. Neilson, W.K. Dawson, F.A. Johnson, Rev. Sci. Instr. 30 (1959) 963.

31 T.K. Fowler, W.M. Good, Nucl. Instr. and Meth. 7 (1960) 245.

L.E. Beghean, M.K. Salomaa, Nucl. Instr. and Meth. 17 (1962) 181.

32 L. Cranberg, R.A. Fernald, F.S. Hahn, E.F. Schrader, Nucl. Instr. and Meth. 12 (1961) 335.

K. Tsukada, S. Tamaka, M. Maruyama, Y. Tomita, Nucl. Instr. and Meth. 39 (1966) 249.

33 W.G. Davies, Ph. D. Thesis, University of Alberta (1966).

34 J.V. Kane, in Nuclear Structure and Electomagnetic Interactions edited by N. Macdonald (Plenum Press, New York, 1965) p. 453.

35 J.F. Whalen, J.W. Meadows, R.N. Larsen, Rev. Sci. Instr. 35 (1964) 682.

36 R.L. Chase, Nuclear Pulse Spectrometry (MacGraw Hill 1961), p. 164.

37 D.A. Gedcke, W.J. Macdonald, Western Region Nuclear Conference, University of Alberta, Edmonton, March, 1966 (unpublished).

38 D.L. Wieber, Nucl. Instr. and Meth. 24 (1963) 269.

39 D.A. Gedcke, "Modifications to TMC Analyser", Nuclear Research Centre (April 1966).

40 M.E. Rose, Phys. Rev. 91 (1953) 610.

41 W.D. Allen, "Flat Response Counters", ch. 3A Fast Neutron Physics, edited by J.B. Marion, J.L. Fowler (Intercience Publishers Inc., New York, 1960).

42 P.R. Bevington, W.W. Roland, H.W. Lewis, Phys. Rev. 121 (1961) 871.

43 S.J. Bame, E. Haddad, J.E. Perry, K.K. Smith, Rev. Sci. Instr. 28 (1957) 997.

44 C.R. Lubitz, Tables of Butler-Born Approximation, University of Rochester (1957).

45 W.R. Smith, Oak Ridge National Laboratory Report ORNL-TM-1151 (1965).

46 C.F. Clement, Phys. Rev. 128 (1962) 2728.

48 H.F. Lutz, J.B. Mason, M.D. Karvelis, Nucl. Phys. 47 (1963) 521.

47 R.N. Maddison, Proc. Phys. Soc. (London) 79 (1962) 264.

49 R.H. Siemssen, M. Cosack, R. Felst, Nucl. Phys. 69 (1965) 209.

50 R. Huby, J.R. Mines, Rev. Mod. Phys. 37 (1965) 406.

51 J.L. Alty, L.L. Green, R. Huby, G.D. Jones, J.R. Mines, J.F. Sharpey-Shafer, Phys. Lett. 20 (1966) 664.

52 G.R. Satchler, (private communication) 1966.

53 A.B. Smith, (private communication) 1966.

54 D.E. Alburger, P.D. Parker, D.J. Bredin, D.H. Wilkinson, P.F. Donovan, A. Gallmann, R.E. Pixley, L.F. Chase Jr., R.E. Macdonald, Phys. Rev. 143 (1966) 692.

55 S. Cohen, D. Kurath, Nucl. Phys. 73 (1965) 1.

56 G.R. Satchler, in DINRM p. 80.

57 L.L. Lee, J.P. Schiffer, B. Zeidman, G.R. Satchler, Phys. Rev. 136 (1964) B971.

58 K.R. Greider, G.L. Strobel, University of California (Davis) Report CNL-UCD 39 (1966).

59 J.B. French, in Nuclear Spectroscopy, Part B Ch. 5G edited by F. Ajzenberg-Selove (Academic Press, New York, 1960).

60 D. Kurath, referred to in Phys. Rev. Lett. 16 (1966) 1050.

D. Kurath, (private communication) 1966.

61 W.R. Smith, Phys. Rev. 137 (1965) B913.

62 J.P. Schiffer, in Proceedings of the Summer Study Group on the Physics of the Emperor Tandem Van de Graaff Region, Brookhaven National Laboratory Report BNL (C-46) (1965) p. 455

63 W.T. Pinkston, G.R. Satchler, Nucl. Phys. 72 (1965) 641.

64 M.J. Hooper, L.B.J. Goldfarb, Phys. Lett. 4 (1963) 148.

65 A. Elwyn, J.V. Kane, S. Ofer, D.H. Wilkinson, Phys. Rev. 116 (1959) 1490.

66 P. Goldhammer, Rev. Mod. Phys. 35 (1963) 40 - 107.

67 W.B. Reid, R.H. Hummel, Can. Nuclear Technology January-February 1966.

68 T. Lauritson, F. Ajzenberg-Selove, Nucl. Phys. 78 (1966) 1.

69 J. Tepel, Nucl. Instr. and Meth. 40 (1966) 100.

APPENDIX A. THE TIME-SHIFT CORRECTION

The origin of time-shift is easily understood if one considers fig. A [36]). This figure shows how signal timing is dependent on

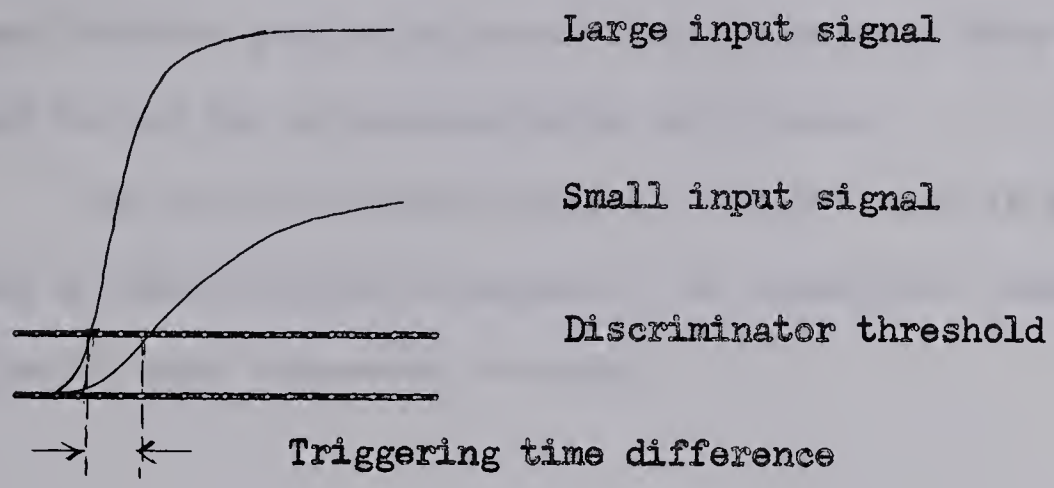

Fig. A

pulse amplitude because of the finite discriminator threshold. The finite bias is necessary to avert triggering on random noise fluctuations.

To correct for this time shift in our case, the amplitude of the signal from the principal neutron detector is recorded by the computer simultaneously with the neutron time signal. Subsequently a channel shift dependent on the recorded detector signal amplitude is applied to the neutron count.

The appropriate channel shift is determined prior to the experiment by analysis of a two-dimensional 4096 channel record of the mono-energetic neutron group from a reaction such as $T(p,n)^3He$, or $D(d,n)^3He$. One dimension corresponds to the detector signal amplitude,

which is divided into thirty-two groups or bins of pulse height, the second dimension to the ordinary time or energy spectrum of the neutrons.

Thus a display of the 4096 data channels gives thirty-two time spectra of 128 channels each, with the neutron peak successively time-shifted from bin to bin. CORR, a subroutine of GPKS, can then compute the channel shift appropiate to each bin by determining the centroid of each neutron peak relative to a standard peak. Zero channel shift refers to the bin of maximum pulse amplitudes.

The table of channel shifts is then stored in memory and during a time-of-flight experiment, the appropiate channel shift is applied to each time-event recorded.

APPENDIX B

This appendix contains relative angular distributions for the $^{9}Be(d,n)^{10}B$ and $^{16}O(d,n)^{17}F$ reactions at deuteron bombarding energy Ed = 5.54 MeV. There are fourteen neutron distributions for the $^{9}Be(d,n)^{10}B$ reaction corresponding to ^{10}B excitations up to 7.00 MeV. The two distributions for the $^{16}O(d,n)^{17}F$ reaction correspond to excitation of the ground and 0.5 MeV states of ^{17}F.

ANGULAR DISTRIBUTION OF THE 0.00 MeV STATE OF

^{10}B FROM $^{9}Be(d,n)^{10}B$ AUG. 18/65

Angle (C of M)	Corrected Area	Error
0.000	0.00826	0.00079
5.539	0.01121	0.00085
11.074	0.01520	0.00120
16.601	0.01977	0.00161
22.116	0.02930	0.00181
27.615	0.02778	0.00192
33.094	0.02383	0.00160
38.550	0.02068	0.00148
49.377	0.01186	0.00081
65.362	0.00739	0.00059
80.981	0.00650	0.00049
106.096	0.00533	0.00039
115.815	0.00769	0.00057
125.357	0.00956	0.00062
139.371	0.00921	0.00060
153.089	0.00891	0.00065

ANGULAR DISTRIBUTION OF THE 0.717 MeV STATE OF

^{10}B FROM $^{9}Be(d,n)^{10}B$ AUG. 18/65

Angle (C of M)	Corrected Area	Error
0.000	0.01229	0.00097
5.562	0.01566	0.00103
11.120	0.02026	0.00141
16.669	0.02533	0.00185
22.206	0.03655	0.00207
27.726	0.03809	0.00233
33.225	0.03008	0.00183
38.700	0.02544	0.00165
49.563	0.01111	0.00075
65.590	0.00413	0.00042
81.236	0.00389	0.00038
106.356	0.00360	0.00031
116.063	0.00373	0.00039
125.585	0.00363	0.00037
139.557	0.00354	0.00037
153.220	0.00532	0.00053

ANGULAR DISTRIBUTION OF THE 1.74 MeV STATE OF

^{10}B FROM $^{9}Be(d,n)^{10}B$ AUG. 18/65

Angle (C of M)	Corrected Area	Error
0.000	0.00464	0.00049
5.600	0.00528	0.00052
11.196	0.00581	0.00050
16.783	0.00589	0.00058
22.356	0.00878	0.00068
27.912	0.00729	0.00059
33.446	0.00564	0.00055
38.953	0.00408	0.00040
49.875	0.00174	0.00030
65.973	0.00114	0.00023
81.664	0.00119	0.00023
106.792	0.00052	0.00017
116.479	0.00068	0.00017
125.968	0.00084	0.00021
139.869	0.00114	0.00030
153.441	0.00086	0.00027

ANGULAR DISTRIBUTION OF THE 2.15 MeV STATE OF

^{10}B FROM $^{9}Be(d,n)^{10}B$ AUG. 18/65

Angle (C of M)	Corrected Area	Error
0.000	0.00408	0.00048
5.618	0.00474	0.00048
11.232	0.00486	0.00044
16.836	0.00514	0.00054
22.426	0.00878	0.00067
27.998	0.00887	0.00063
33.548	0.00746	0.00061
39.071	0.00514	0.00043
50.020	0.00444	0.00041
66.151	0.00357	0.00033
81.862	0.00319	0.00031
106.995	0.00251	0.00025
116.672	0.00360	0.00028
126.146	0.00345	0.00030
140.014	0.00455	0.00047
153.543	0.00388	0.00037

ANGULAR DISTRIBUTION OF THE 3.58 MeV STATE OF

^{10}B FROM $^{9}Be(d,n)^{10}B$ AUG. 18/65

Angle (C of M)	Corrected Area	Error
0.000	0.01304	0.00080
5.696	0.01361	0.00093
11.386	0.01276	0.00093
17.066	0.01007	0.00086
22.730	0.01137	0.00073
28.375	0.01077	0.00071
33.993	0.00835	0.00047
39.582	0.00719	0.00052
50.651	0.00660	0.00046
66.925	0.00566	0.00047
82.727	0.00516	0.00033
107.877	0.00452	0.00029
117.513	0.00520	0.00040
126.921	0.00566	0.00035
140.645	0.00439	0.00027
153.988	0.00412	0.00037

ANGULAR DISTRIBUTION OF THE 4.77 MeV STATE OF

^{10}B FROM $^{9}Be(d,n)^{10}B$ AUG. 18/65

Angle (C of M)	Corrected Area	Error
0.000	0.00546	0.00065
5.789	0.00640	0.00058
11.572	0.00500	0.00059
17.343	0.00543	0.00061
23.097	0.00507	0.00052
28.828	0.00608	0.00044
34.530	0.00585	0.00044
40.198	0.00551	0.00040
51.412	0.00630	0.00050
67.860	0.00596	0.00040
83.772	0.00657	0.00047
108.943	0.00580	0.00046
118.529	0.00638	0.00057
127.855	0.00752	0.00043
141.406	0.00487	0.00032
154.525	0.00293	0.00037

ANGULAR DISTRIBUTION OF THE 5.11 MeV STATE OF

^{10}B FROM $^{9}Be(d,n)^{10}B$ AUG. 18/65

Angle (C of M)	Corrected Area	Error
0.000	0.16293	0.00379
5.823	0.14526	0.00482
11.641	0.08374	0.00464
17.446	0.05399	0.00298
23.233	0.03440	0.00179
28.995	0.01597	0.00105
34.728	0.00834	0.00070
40.426	0.00769	0.00066
51.694	0.00976	0.00083
68.206	0.01053	0.00058
84.159	0.00791	0.00052
109.337	0.00301	0.00038
118.905	0.00422	0.00039
128.201	0.00458	0.00041
141.688	0.00000	0.00000
154.723	0.00183	0.00018

ANGULAR DISTRIBUTION OF THE 5.16 MeV STATE OF

^{10}B FROM $^{9}Be(d,n)^{10}B$ AUG. 18/65

Angle (C of M)	Corrected Area	Error
0.000	0.02044	0.00200
5.829	0.02168	0.00212
11.652	0.03524	0.00362
17.462	0.02818	0.00242
23.254	0.01622	0.00139
29.022	0.01127	0.00097
34.760	0.00751	0.00067
40.462	0.00656	0.00064
51.738	0.00433	0.00073
68.261	0.00171	0.00034
84.220	0.00171	0.00034
109.400	0.00262	0.00037
118.965	0.00198	0.00034
128.256	0.00696	0.00068
141.733	0.00001	0.00001
154.755	0.00159	0.00041

ANGULAR DISTRIBUTION OF THE 5.93 MeV STATE OF

$^{9}Be(d,n)^{10}B$ AUG. 18/65 GAUSS-FITTED

Angle (C of M)	Corrected Area	Error
0.000	0.04674	0.00371
5.930	0.04342	0.00362
11.852	0.03860	0.00321
17.762	0.03860	0.00306
23.650	0.03908	0.00310
29.512	0.02870	0.00184
35.340	0.01953	0.00125
41.129	0.01397	0.00146
52.562	0.00730	0.00060
69.274	0.00462	0.00045
85.354	0.00497	0.00042
110.556	0.00256	0.00039
120.066	0.00279	0.00035
129.269	0.00357	0.00044
142.557	0.00389	0.00058
155.335	0.00348	0.00056

ANGULAR DISTRIBUTION OF THE 6.02 MeV STATE OF

^{10}B FROM $^{9}Be(d,n)^{10}B$ AUG. 18/65

Angle (C of M)	Corrected Area	Error
0.000	0.00760	0.00085
5.944	0.00677	0.00097
11.881	0.00479	0.00066
17.805	0.00450	0.00082
23.708	0.00464	0.00077
29.583	0.00435	0.00088
35.424	0.00296	0.00069
41.225	0.00164	0.00082
52.682	0.00176	0.00045
69.421	0.00286	0.00044
85.518	0.00001	0.00001
110.723	0.00163	0.00036
120.226	0.00192	0.00033
129.416	0.00200	0.00037
142.676	0.00142	0.00043
155.419	0.00034	0.00033

ANGULAR DISTRIBUTION OF THE 6.14 MeV STATE OF

^{10}B FROM $^{9}Be(d,n)^{10}B$ AUG. 18/65

Angle (C of M)	Corrected Area	Error
0.000	0.0117	0.0006
5.965	0.0112	0.0006
11.923	0.0118	0.0007
17.867	0.0132	0.0007
23.790	0.0132	0.0006
29.685	0.0132	0.0008
35.545	0.0115	0.0006
41.364	0.0124	0.0012
52.854	0.0097	0.0006
85.755	0.0045	0.0004
110.965	0.0029	0.0004
120.456	0.0026	0.0004
129.628	0.0029	0.0005
142.848	0.0020	0.0005
155.540	0.0012	0.0004

ANGULAR DISTRIBUTION OF THE 6.57 MeV STATE OF

^{10}B FROM $^{9}Be(d,n)^{10}B$ AUG. 18/65

Angle (C of M)	Corrected Area	Error
0.000	0.0078	0.0022
6.050	0.0058	0.0023
12.092	0.0063	0.0015
18.118	0.0093	0.0024
24.122	0.0127	0.0011
30.096	0.0156	0.0009
36.032	0.0156	0.0009
41.924	0.0168	0.0009
53.546	0.0140	0.0009
70.485	0.0071	0.0011
86.709	0.0031	0.0004
111.939	0.0052	0.0017
121.383	0.0000	0.0002
130.480	0.0025	0.0008
143.540	0.0001	0.0014
156.027	0.0000	0.0006

ANGULAR DISTRIBUTION OF THE 6.88 MeV STATE OF

^{10}B FROM $^{9}Be(d,n)^{10}B$ AUG. 18/65

Angle (C of M)	Corrected Area	Error
0.000	0.0025	0.0008
6.127	0.0029	0.0006
12.247	0.0017	0.0006
18.350	0.0014	0.0006
24.428	0.0011	0.0004
30.474	0.0012	0.0003
36.481	0.0015	0.0002
42.439	0.0001	0.0001
54.184	0.0009	0.0003
71.271	0.0005	0.0002
87.590	0.0000	0.0000
112.838	0.0000	0.0000
122.239	0.0001	0.0002
131.266	0.0000	0.0000
144.178	0.0000	0.0000

ANGULAR DISTRIBUTION OF THE 7.01 MeV STATE OF

^{10}B FROM $^{9}Be(d,n)^{10}B$ AUG. 18/65

Angle (C of M)	Corrected Area	Error
0.000	0.0049	0.0009
6.166	0.0035	0.0006
12.323	0.0047	0.0007
18.463	0.0044	0.0007
24.578	0.0023	0.0004
30.660	0.0013	0.0003
36.701	0.0009	0.0002
42.692	0.0010	0.0003
54.498	0.0000	0.0000
71.658	0.0002	0.0002
88.024	0.0000	0.0000
113.280	0.0001	0.0001
122.661	0.0000	0.0000
131.653	0.0000	0.0000
144.492	0.0000	0.0000

ANGULAR DISTRIBUTION OF THE 0.00 MeV STATE OF

^{17}F FROM $^{16}O(d,n)^{17}F$ DEC. 8/65

Angle (C of M)	Corrected Area	Error
0.000	0.1181	0.0059
5.530	0.1259	0.0067
11.057	0.1680	0.0088
16.575	0.2267	0.0118
22.082	0.2686	0.0140
27.572	0.3133	0.0163
33.044	0.3285	0.0172
38.492	0.3058	0.0160
49.306	0.2272	0.0119
65.276	0.1014	0.0056
80.886	0.0446	0.0026
96.094	0.0350	0.0021
106.001	0.0276	0.0017
115.725	0.0522	0.0031
125.274	0.0580	0.0035
139.304	0.0537	0.0033
153.042	0.0532	0.0033
5.530	0.1260	0.0067

ANGULAR DISTRIBUTION OF THE 0.50 STATE OF

^{17}F FROM $^{16}O(d,n)^{17}F$ DEC. 8/65

Angle (C of M)	Corrected Area	Error
0.000	1.2908	0.0690
5.576	1.1861	0.0634
11.148	0.9084	0.0486
16.711	0.5937	0.0319
22.262	0.3206	0.0173
27.795	0.1534	0.0084
33.307	0.0769	0.0043
38.794	0.0549	0.0031
49.679	0.0884	0.0049
65.734	0.1010	0.0058
81.397	0.0725	0.0043
96.623	0.0372	0.0023
106.522	0.0180	0.0012
116.222	0.0276	0.0018
125.732	0.0221	0.0015
139.677	0.0184	0.0013
153.305	0.0141	0.0010
5.576	1.1314	0.0606

APPENDIX C

The use of the time-of-flight system to determine target thickness.

The feasibility of estimating target thickness by means of the neutron time-of-flight spectrometer has been investigated. To this end thin- and thick-target yields of neutrons from the $^{16}O(d,n_1)^{17}F$ transition were studied at 3.50 MeV deuteron energy.

The thin target has already been described in section 2.4, and consisted of a thin film of ^{9}Be deposited on a Molybdenum foil. The ^{16}O contamination is evident in the $^{9}Be(d,n)^{10}B$ spectrum of fig. 3. At 0^{o}, the neutron peak corresponding to the first excited state of ^{17}F (0.5 MeV excitation) is not contaminated by neutrons corresponding to ^{10}B states.

The thick target consisted of a small foil of Zirconium canning material used in one of the Chalk River reactors. The surface of this material had been oxidised by Oxygen-16 and Oxygen 17, and a request had been made for some estimate of the depth of Oxygen penetration into the Zirconium surface.

If the electronic resolution of the time-of-flight spectrometer is very good, then the shape of the neutron peak for the $^{16}O(d,n_1)^{17}F$ reaction should reflect the distribution of the ^{16}O in the target. The fastest neutrons will come from the surface layers of the target, and will hence have the shortest flight times. As the deuterons penetrate the target they lose energy by ionisation of the target atoms and will thus give rise

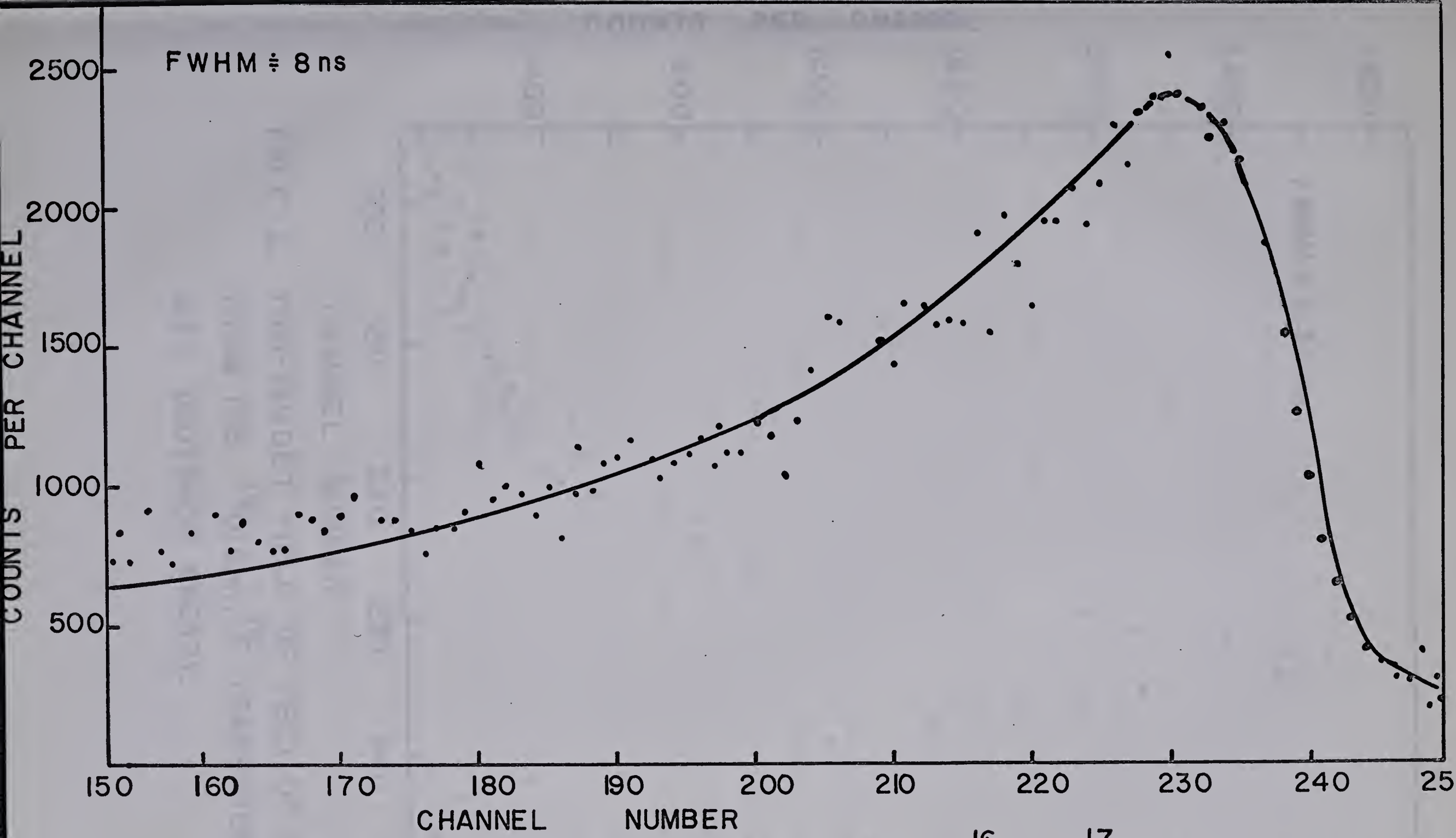

FIG. C-1. THICK-TARGET YIELD OF NEUTRONS FROM THE $^{16}O(d,n_1)^{17}F$ TRANSITION AT 3·5MEV DEUTERON ENERGY. THE SMOOTH CURVE WAS CALCULATED AS DESCRIBED IN THE TEXT WITH THE DECAY PARAMETER $\alpha = 9300\ cm^{-1}$. A CONSTANT BACKGROUND OF 250 COUNTS WAS ALLOWED FOR IN THE CALCULATION.

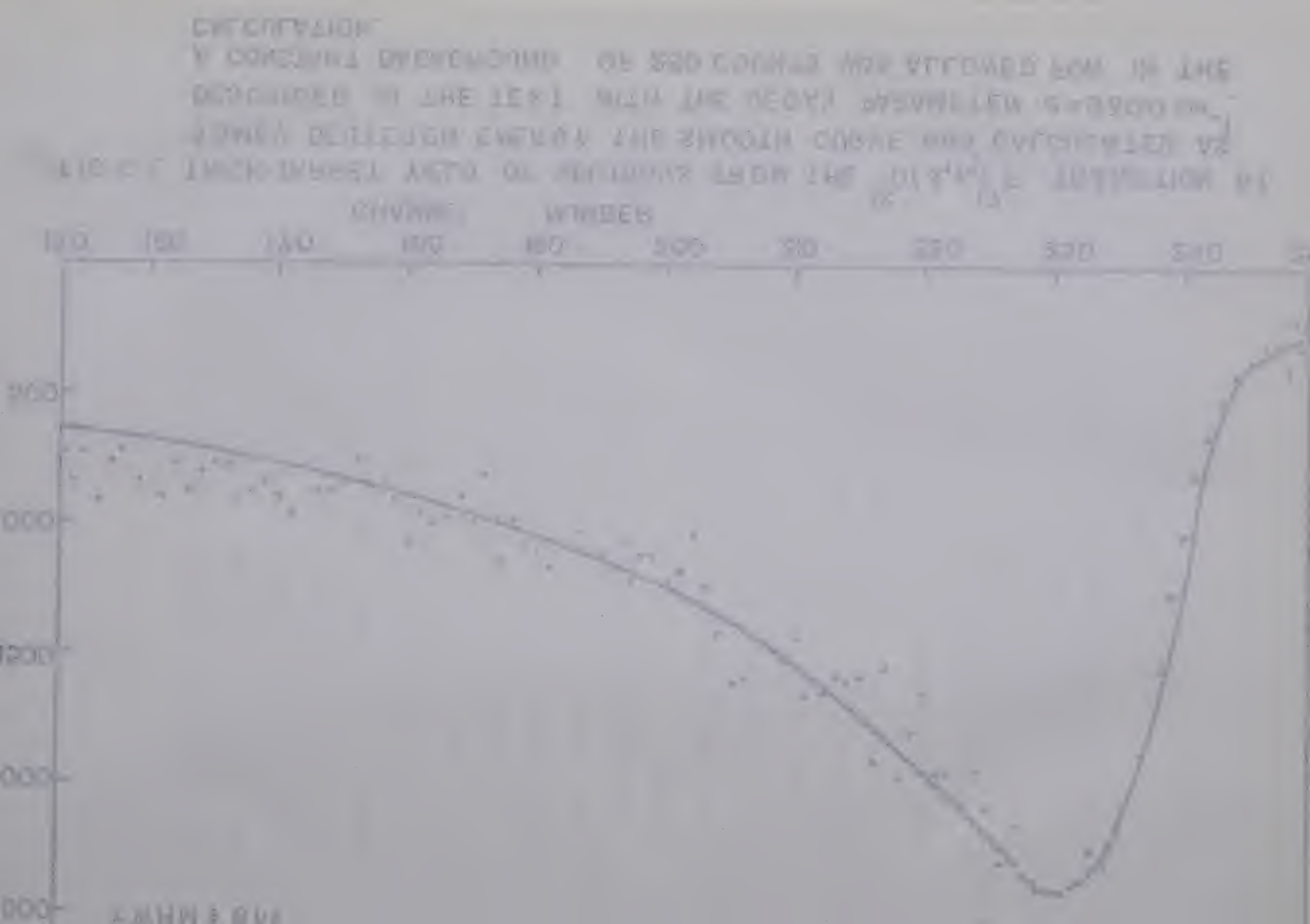

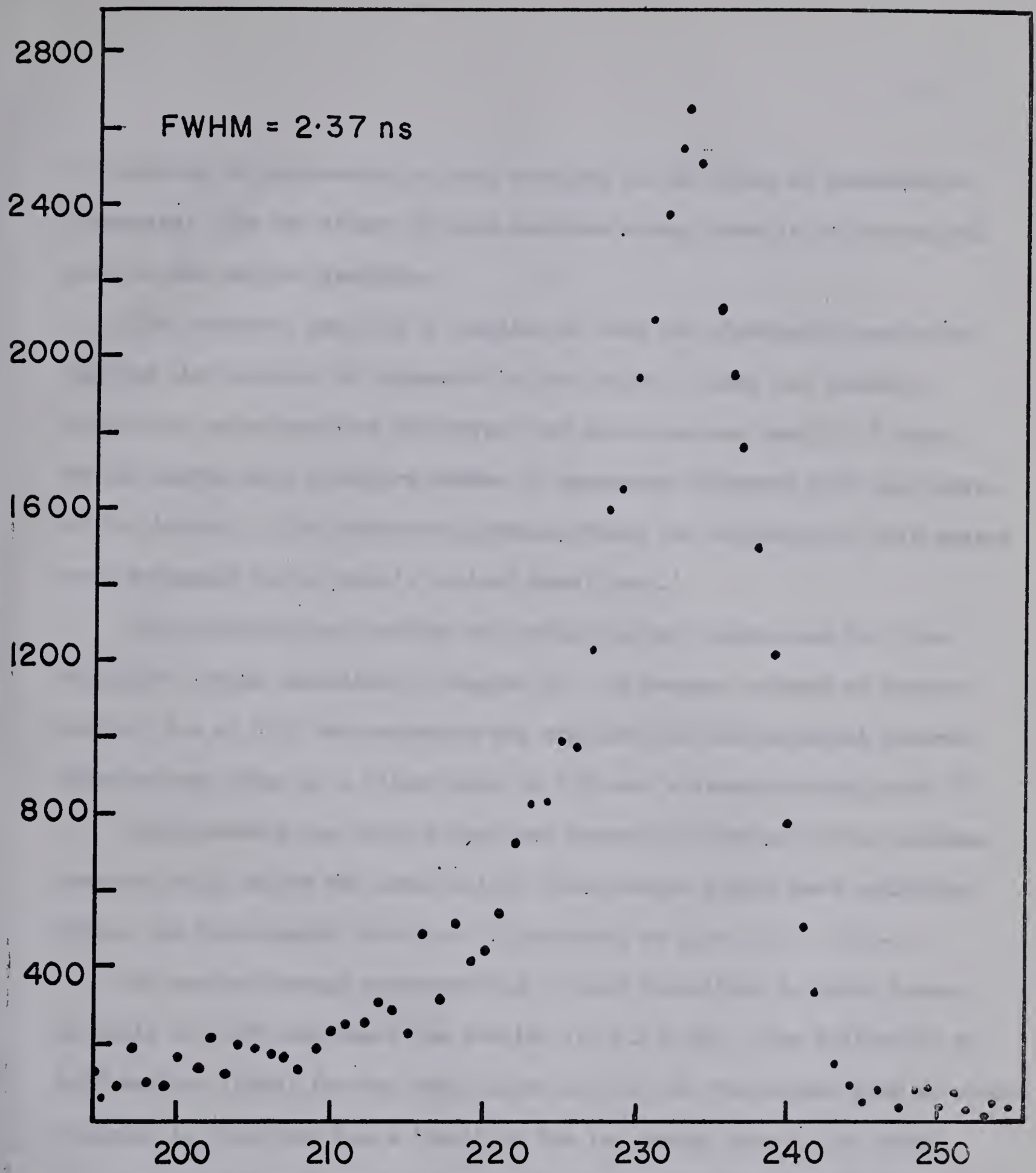

FIG C-2. THIN-TARGET YIELD OF YIELD OF NEUTRONS FROM THE $^{16}O(d,n_1)^{17}F$ TRANSITION AT 3·5 MEV DEUTERON ENERGY.

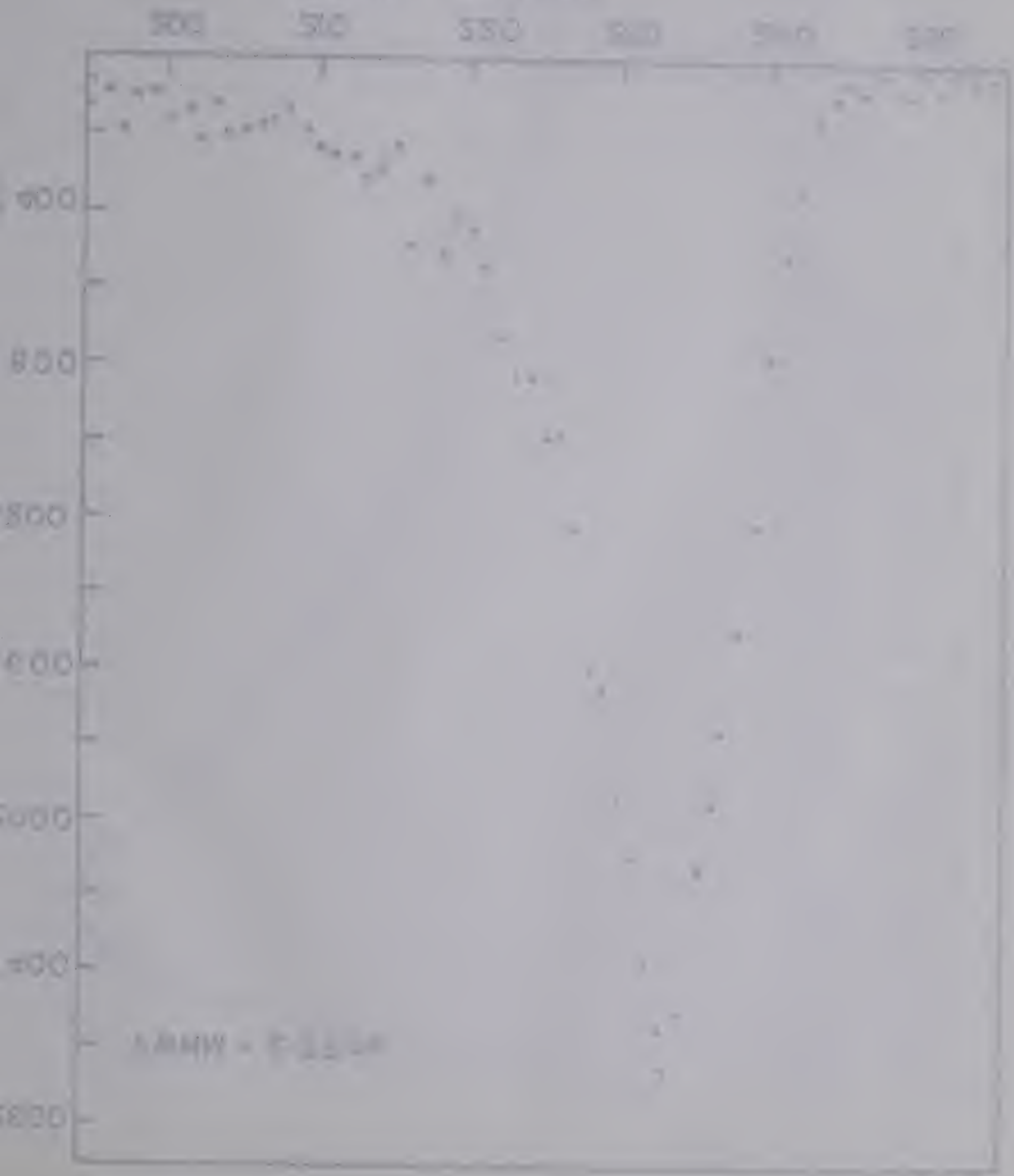

to neutrons of progressively lower energies as the depth of penetration increases. The net effect of this deuteron energy loss is to broaden the peak in the neutron spectrum.

The broadened shape is a function of both the electronic resolution and the distribution of Oxygen-16 in the target. Since the deuteron absorption cross-sections for Oxygen and Zirconium are small (< 1 barn) we can assume that a uniform number of deuterons interacts with all layers of the target. (The absorption cross-sections for deuterons of this energy were estimated using Perey's optical model code.)

The experiment was carried out using the two targets and the time-of-flight system described in Chapter II. An average current of approximately 1μA of 3.50 MeV deuterons was employed and the principal neutron detector was fixed at a flight path of 6.3m and a laboratory angle of 0^{o}.

Unfortunately the thick target was seriously affected by the deuteron beam and only one or two satisfactory thick target yields were collected. Thick- and thin-target yields are illustrated in figs. C-2, and C-1.

The neutron energy corresponding to this transition is given kinematically as 1.229 MeV where the Q-value is -2.131 MeV. The full-width at half-maximum (FWHM) for the thin target is 2.37 ns. The latter peak is almost Gaussian in shape but has a 'tail' on the low energy side of the peak.

The thick target peak is broadened considerably to about 8ns FWHM. It is evident from the asymmetric shape that the distribution of ^{16}O in the target is a non-linear function of the depth. If the ^{16}O had been uniform, a roughly rectangular peak shape should result.

If the delays introduced by the target energy losses are negligible then the neutron peak represents the intrinsic resolution curve of the electronics, P(t), where t is the flight time. If there is a measurable energy loss due to target thickness, then one obtains the delayed curve F(t). One can write

$$F(t) = \int_{-\infty}^{\infty} f(t') . P(t-t') dt'$$

where $f(t')$ is related to the distribution of ^{16}O atoms in the target associated with flight time t', and this function is the object of interest.

If we can assume that P(t) is given by the thin target curve, then we can take some functional form for f(t), and numerically integrate to find F(t). As a first approximation, it was decided to try an exponential distribution for the target atoms. Thus the number of ^{16}O atoms in $(x, x+dx)$ is $\text{const.}\exp(-\alpha(x))dx$ where x is the depth coordinate measured normal to the target surface. For the reaction under study, the depth x, and the flight time are related kinematically as

$$x \doteq \frac{2.27.10^5}{|dE_d/dx|} \left(1/t_o^2 - 1/t^2\right) \text{ cm}$$

where t_o is the flight time in ns for a 1.229 MeV neutron over a 6.3m flight path (=410.5ns);

t is the flight time in ns for a neutron coming from depth x in the target;

$|dE_d/dx|$ is the tabulated target energy loss in units of MeV/cm. (This quantity has been assumed constant in deriving the above formula.)

The tables of Coon (ref. C) gave

$$\left|dE_d/dx\right| = 101 \text{ keV}.\text{mg}^{-1}.\text{cm}$$

Thus

$$\exp(-\alpha x)dx = \frac{\exp\left(-2.21.\alpha.10^{-3}.(1 - 1/(1 + t/410.5)^2)\right)dt}{(410.5 + t)^3}$$

For convenience it was decided to take a Gaussian form for P(t) with a standard deviation estimated from curve C-1. This leads to

$$F(t) = \int_0^\infty \frac{\exp(-0.466(t-t')^2 - 2.21.\alpha.10^{-3}.(1 - 1/(1 + t'/410.5)^2))dt'}{(410.5 + t')^3}$$

The distribution function $f(t') = 0$ for $t' < 0$, and this condition fixes the integration limits.

The above integral for F(t) was computed numerically for several values of α, until a reasonable fit to the asymmetric experimental shape was obtained. The results of one such calculation for $\alpha = 9300\text{cm}^{-1}$ are indicated in fig. C-2. Acceptable agreement with the shape could be obtained for values of α within $\pm$ 15% of the above, at least for about 60 channels from the peak channel. Thereafter the theoretical shape underestimated the experimental counts. This discrepancy may be due to any one of a number of effects including contributions from the tail of the experimental P(t) or breakdown of the assumption of an exponential distribution of target atoms. However the agreement over most of the curve tends to support the latter assumption, which can also be justified on physical grounds if the target was formed by a diffusion of ^{16}O atoms into

a pure Zirconium surface. With the estimated value of $\alpha(9300cm^{-1})$ the number of target atoms drops to half the number at the surface at a depth of about 7500 angstroms.

In conclusion this rough analysis appears to show that it is possible to obtain some idea of the distribution of target atoms from the shape of the associated neutron peak. As a method of estimating target thickness it holds promise although more experimentation and analysis is necessary to place the technique on a firmer basis.

REFERENCES

C J.H. Coon, in Fast Neutron Physics Vol. 1 (edited by J.B. Marion and J.L. Fowler, Interscience Publishers Inc., New York, 1960) p. 677